Preclinical Testing of a Novel Niclosamide Stearate Prodrug Therapeutic (NSPT) shows efficacy against Osteosarcoma

Gireesh B. Reddy, MD[1†] and David L. Kerr, MD[2†], Ivan Spasojevic, PhD[3,4], Artak Tovmasyan, PhD[3], David Hsu, MD, PhD[3,4], Brian E. Brigman, MD, PhD[2,3], Jason A. Somarelli PhD[3,4], David Needham PhD[3,5,6], William C. Eward, DVM, MD[2,3]

[1]Duke University School of Medicine, Durham, NC, [2]Department of Orthopaedic Surgery, Duke University Medical Center, Durham, NC, [3]Duke Cancer Institute, Durham, NC, [4]Department of Medicine, Duke University, Durham, NC, [5]Department of Mechanical Engineering and Material Science, Duke University, [6] School of Pharmacy, University of Nottingham, Nottingham UK.

[†]Gireesh B. Reddy and David L. Kerr are co-first authors.

Corresponding Author:

William C. Eward DVM, MD
Associate Professor of Orthopaedic Surgery
Section of Orthopaedic Oncology
Duke University, Durham, NC, USA
Address: Box 3312 DUMC, Durham, NC 27710
Email: w.eward@alumni.duke.edu
Telephone: 919.681.6982

Conflict of Interest Statement: The authors whose names are listed above certify that they have NO affiliations with or involvement in any organization or entity with any financial or non-financial interests in the subject matter or materials discussed in this manuscript.

Statement of Translational Relevance

This investigation of the niclosamide prodrug nanoparticle as a potential treatment for osteosarcoma (OS) represents a foundation for additional preclinical and clinical studies. In the drug development arena, the ability of the prodrug nanoparticle to significantly increase the bioavailability of a previously potent, but clinically unusable drug, marks a significant advancement in the conversion of niclosamide to clinical use. Furthermore, the formulation may be useful for other hydrophobic drugs that have stagnated in preclinical testing due to poor bioavailability and limited *in vivo* stability, despite promising *in vitro* results. In the chemotherapy arena, the NSPT demonstrates efficacy against multiple human and canine OS cell lines and different signaling pathways. Given the challenges in developing targeted therapies for OS and other genetically heterogeneous tumors, NSPTs in particular may have potential utility for an effective treatment that avoids the toxicity that has challenged OS patient populations both during and after current standard-of-care cytotoxic therapies.

Abstract

Therapeutic advances for osteosarcoma (OS) have stagnated over the past several decades, leading to an unmet clinical need for patients. The purpose of this study was to develop a novel therapy for OS by reformulating and validating niclosamide, an established anthelminthic agent, as a Niclosamide Stearate Prodrug Therapeutic (NSPT). We sought to improve the low and inefficient clinical bioavailability of oral dosing, especially for the relatively hydrophobic classes of anti-cancer drugs. Nanoparticles were fabricated by rapid-solvent shifting and verified using dynamic light scattering and UV-vis spectrophotometry. NSPT efficacy was then studied *in vitro* for cell-viability, cell-proliferation, intracellular-signaling by western blot; *ex vivo* pulmonary metastatic assay model; and *in vivo* PK and lung mouse metastatic model of OS. NSPT formulation stabilizes niclosamide stearate against hydrolysis and delays enzymolysis; increases circulation in vivo with $t_{1/2}$ ~5 h; reduces cell-viability and cell-proliferation in human and canine OS cells in vitro at 0.2 – 2 μM IC_{50}; inhibits recognized growth pathways, and induces apoptosis at 20μM; eliminates metastatic lesions in the ex-vivo lung metastatic model; and, when injected intravenously (i.v.) at 50mg/kg weekly, it prevents metastatic spread in the lungs in a mouse model of OS over 30 days. In conclusion, niclosamide was optimized for preclinical drug delivery as a unique prodrug nanoparticle injected i.v. at 50mg/kg (1.9mM). This increased bioavailability of niclosamide in the blood stream prevented metastatic disease in the mouse. This chemotherapeutic strategy is now ready for canine trials, and if successful, will be targeted for human trials in OS patients.

1. Introduction

1.1 OS has seen almost no chemotherapeutic advances over the past three decades

OS is the most common primary bone malignancy in humans. It most frequently occurs in adolescence (Friebele, Peck et al. 2015). At presentation, 15 – 20% of patients already have visible pulmonary metastatic disease, and a majority of patients have lung metastases that are not yet detectable (Taran, Taran et al. 2017). Because most patients without visible metastatic disease at presentation likely have undetectable micro-metastasis, systemic therapy - both neoadjuvant and adjuvant therapy – is a critical addition to surgical resection (Biermann, Chow et al. 2017). Sadly, OS, unlike most other solid tumors, has seen relatively few chemotherapeutic advances over the past three decades, particularly with respect to patients presenting with advanced or metastatic disease (Kager, Zoubek et al. 2003, Mialou, Philip et al. 2005, Aljubran, Griffin et al. 2009, Mirabello, Troisi et al. 2009, Crawford 2013). Indeed, OS is one of the only types of cancer for which the prognosis given today is nearly identical to the prognosis given in 1988 (Kansara, Teng et al. 2014). Furthermore, the standard-of-care chemotherapy regimen of Methotrexate, Adriamycin (doxorubicin), and cis-Platin (MAP) is based on cytotoxic agents associated with substantial treatment-derived morbidity (Ferrari, Ruggieri et al. 2012, Whelan, Bielack et al. 2014, Marina, Smeland et al. 2016). Although chemotherapeutic sequela can prematurely delay or abort treatment regimens in pediatric and adolescent patients, more severe complications such as anthracycline-induced cardiomyopathy greatly increase subsequent morbidity (Nagarajan, Kamruzzaman et al. 2011, Taran, Taran et al. 2017). Indeed, even OS survivors do not have a normal life expectancy due to the morbidity from their adolescent therapy. Given the extensive toxicity of these agents, there is a critical need to identify new therapeutics with lower systemic-toxicity and greater efficacy to treat OS with better outcomes and less treatment-derived morbidity.

1.2 Repurposing Niclosamide for anti-cancer applications

Since around 2010, there has been a steady rise in popularity of studies investigating niclosamide for a range of diseases (Kadri, Lambourne et al. 2018), including Parkinson's, diabetes, bacterial and viral infections, and cancer. Niclosamide, an FDA-approved anthelmintic (Perera, Western et al. 1970, WHO 2017), has recently attracted considerable interest as a novel antitumor agent (Jin, Lu et al. 2010, Osada, Chen et al. 2011, Pan, Ding et al. 2012, Arend, Londoño-Joshi et al. 2013, Londono-Joshi, Arend et al. 2014). Pharmaceutically, niclosamide has been shown to be a very "dirty drug"; it inhibits (at least) 17 different pathways in cancer cells (Pan, Ding et al. 2012, Li, Li et al. 2014). In the context of OS, niclosamide inhibits multiple pathways that promote survival and growth that are known to be dysregulated in OS, including the Wnt/ß-catenin, Akt/mTOR/PI3K, JAK/STAT, NOTCH, and NF-κB pathways (Chen, Wang et al. 2009, Arend, Londoño-Joshi et al. 2013, Li, Li et al. 2014, Ahmed, Shaw et al. 2016, Suliman, Zhang et al. 2016).

In vitro studies have shown that niclosamide induces cell cycle arrest in G_1/G_0 with cell viability IC_{50}s in the 100s of nM to low μM range (Arslanagic, Hervella et al. 2016, Arslanagic-Kabiljagic 2019, Karimi 2019 (exp)). In fact, *in vitro* studies of niclosamide with the NCI-60 human cancer cell lines indicate that niclosamide inhibits cell growth in all tested cancer cell lines (NCI 2014).

In OS, niclosamide also inhibits cell cycle progression (Li, Yu et al. 2015, Liao, Nan et al. 2015), and one of its main mechanisms of cell death seems to be induction of apoptosis (So Jung, lt et al. 2011, Ye, Xiong et al. 2014, Li, Yu et al. 2015). With limited formulations for preclinical evaluation, few studies have been conducted with this drug against cancer *in vivo*. Importantly though, in direct contrast to conventional chemotherapies, *in vitro*, niclosamide is relatively non-toxic to healthy cells [22], including fibroblasts, normal mammary epithelial cells (MCF-10A), and peripheral blood mononuclear cells (PBMCs) (Osada, Chen et al. 2011), and shows no evidence of causing developmental toxicity, mutagenicity or carcinogenicity when taken orally (EPA 1999). Indeed, few, if any, anti-cancer compounds exhibit such a low-toxicity/high-efficacy profile and hit so many different cell targets.

1.3 Inefficient Clinical Bioavailability of Oral Dosing

One of the most important problems in drug delivery to tumors remains is the low and inefficient clinical bioavailability of oral dosing, especially for the many hydrophobic classes of anti-cancer drugs. This is compounded by the fact that there is a dearth of truly-effective formulation options even for preclinical validation that provide high-plasma-concentration-dosing. What is needed for any preclinical validation is an i.v. injectable formulation that puts considerable bioavailable amounts of such drugs in the circulation. Only then can the highly insoluble drug (in our case niclosamide) reach the cancer cells by one or more of several mechanisms and have its intended effects *in vivo*.

For example, in its anthelmintic application, niclosamide is taken orally at doses as much as two grams per patient (veterinary or human) (WHO 2002) and has acute oral LD50 values of >1000 mg/kg (Toxicity Category III, slightly toxic and slightly irritating). Niclosamide is a BCS class II drug, meaning it has poor water solubility (4 μM at pH 7.4, (Ebbesen MF 2019)) and its intestinal absorption is rate-limited by dissolution. Due to this inherently poor aqueous solubility niclosamide has an extremely low systemic bioavailability in the blood stream and thus has extremely low bioavailability that hampers its repurposing in cancer.

Experience with its oral formulation for worms and consideration of its physicochemical properties (logP 4.5, Sw 4 μM) suggests that, in its current tablet-formulation, it is actually not suitable for clinical administration for cancer in order to achieve efficacious results. Indeed, in a recent human prostate-cancer clinical trial the short-lived plasma concentrations that were achieved at the maximum oral-dosing (500 mg given three-times-daily) were only in the range, 35.7 - 82 ng/mL (0.1 – 0.25 μM) (Schweizer, Haugk et al. 2018). These values that were only ~0.014% of the ingested dose were below the therapeutic threshold of 0.5 μM for colony formation, as measured for LNCaP prostate cancer cell studies *in vitro* (Liu, Lou et al. 2015). Clinically, there were no PSA declines in any enrolled subject and the Data Safety Monitoring Board closed the study for futility. Similarly, in a new on-going clinical phase I study in patients with resectable colon cancer (Morse 2017), niclosamide is still being given as the low-bioavailability oral formulation; it is likely to be a very successful Phase 1 toxicity study, but, in view of the earlier prostate-cancer clinical trial (Schweizer, Haugk et al. 2018), efficacy may well be compromised. Finally, early results reported in a very recent ASCO abstract (Burock, Daum et al. 2018) of a prospective phase II clinical trial of niclosamide in patients with metastasized colorectal cancer (mCRC) (Burock, Daum et al. 2018) progressing under standard

therapy (NIKOLO) indicate that an oral dosing of two grams per patient can achieve median C_{max} plasma levels of 0.665 μg/ml (~2 μM). While encouraging, these are still relatively modest levels that are comparable only to IC_{50}s for cell viability. Importantly, no drug-related toxicities were observed. Thus, the biggest challenge for repurposing niclosamide for cancer is not toxicity, but delivery. The drug must be made much more bioavailable in the blood stream and have a more effective pharmacokinetic profile, including higher plasma-bioavailability concentration and circulation half-life.

1.4 Reformulation of Niclosamide as a Niclosamide Stearate Prodrug Therapeutic (NSPT)

Since all clinical niclosamide has only been dosed orally, the maximum tolerated dose (MTD) has never been determined by i.v. administration directly to the blood stream. Thus, we sought to identify the i.v.-injectable MTD and determine what doses of niclosamide could be directly delivered to cancer cells to improve efficacy in early stage metastatic disease. To do this, we have formulated niclosamide as new Niclosamide Stearate Prodrug Therapeutic (NSPT) (Needham, Arslanagic et al. 2016, Walke, Hervella et al. 2017, Walke 2018, Hervella, Walke et al. 2019). Using this nanoparticle formulation, we have started to address some of the main issues of how to increase the bioavailability of Biopharmaceutical Classification System (BCS) Class II and IV (Mehta 2016) anti-cancer drugs and enable effective validation in preclinical studies, and for subsequent canine (Eward, Steve et al. 2018) and human clinical trials.
Current alternative formulations of niclosamide in preclinical development may be hampered by low percent loading (particularly in micelle and many polymer particles), low dosing, low *in vivo* bioavailability, and inefficient access to the tumor interstitium due to large particle size when tested *in vivo* (Supplemental 1.5). To avoid the low bioavailability route of oral uptake and to improve on existing compromised formulations, nanoparticles are needed that 1) enable direct intravenous injection to increase bioavailability and 2) deliver more drug per particle into the blood stream.

2. Materials and Methods

2.1 Materials

Niclosamide stearate prodrug therapeutics (NSPTs) were created using the following materials and suppliers: niclosamide stearate was synthesized by the Duke Small Molecule Synthesis Facility (https://sites.duke.edu/smsf/facility-overview/); niclosamide anhydrous (Sigma Aldrich, Steinheim, Germany), chloroform stock solutions (DSPC, cholesterol, and DSPE PEG^{2000}; Avanti Polar Lipids, Inc., Alabaster, AL, USA), acetone (≥ 99.8 %; Sigma Aldrich, Steinheim, Germany), absolute ethanol (≥ 99.8 %; VWR Chemicals, Paris, France), chloroform (Rathburn Chemicals Ltd., Walkerburn, UK), buffer solution components (hydrochloric acid, sodium chloride, sodium hydroxide; VWR Chemicals, Paris, France), acetic acid (Fluka, Munich, Germany), sodium phosphate monobasic (Sigma Aldrich, Steinheim, Germany), and Millipure water.

2.2 Preparation of Niclosamide Stearate Prodrug Therapeutic (NSPTs).

As briefly described (Walke, Hervella et al. 2017) and in more detail (Walke 2018, Hervella, Walke et al. 2019), the Niclosamide Stearate Prodrug Therapeutic (NSPT) nanoparticles were made by adapting a rapid solvent-exchange method, (Zhigaltsev 2012, Needham, Arslanagic et al. 2016) to a new prodrug, niclosamide stearate (Needham, Arslanagic et al. 2016, Walke 2018, Hervella, Walke et al. 2019). In this method, an organic solution of niclosamide stearate and lipids (DSPC, Cholesterol, and DSPE-PEG^{2000} in a 45:50:5 ratio) were mixed in a 1:1 equivalent molar ratio in acetone-ethanol and rapidly injected into an excess anti-solvent of ultrapure water. Following classical nucleation theory (Karthika, Radhakrishnan et al. 2016), rapid precipitation spontaneously generates nanoparticles consisting of a core of niclosamide stearate coated with a monolayer of the lipids suspended in a mainly aqueous phase, containing 10% of the initial acetone-ethanol solvents (Needham, Arslanagic et al. 2016, Walke, Hervella et al. 2017, Walke 2018, Hervella, Walke et al. 2019). The size of particles (hydrodynamic diameter) was measured using a Dynamic Light Scattering instrument (Dyna Pro Nanostar, Wyatt Technology, Santa Barbara, CA). The NSPT suspension was stored at 4 ^{o}C until use. The concentration prior to use was verified using UV spectrophotometry (SpectraMax, Molecular Devices, San Jose, CA) by measuring the calibrated absorbance of niclosamide-stearate at 330 nm (See Supplemental 2.2 for detailed low- and high- dosing protocols).

2.3 In-Vitro Stability of NSPT in PBS and Plasma

The chemical stability of NSPT, i.e. hydrolysis of niclosamide-stearate to produce niclosamide was investigated by 37 ^{o}C incubation of 1.8 mM NSPT in (1) PBS, (2) mouse, and (3) human plasma (K_2EDTA). A set of 3 aliquots per time-point of each medium was prepared on ice, placed into pre-equilibrated rack/water bath in 37 ^{o}C incubator, and aliquots taken from incubator and placed on dry ice at: 1 min (“zero”), 15 min, 30 min, 1 h, 2 h, 4 h, 8 h, and 24 h. Concentration of both niclosamide-stearate and niclosamide was measured by HPLC as described below.

2.4 Pharmacokinetics (PK) of NSPTs

Analysis of chemical composition were performed by high-performance liquid chromatography (HPLC) for niclosamide and niclosamide stearate up to 24 hours after incubation in PBS buffer, mouse and human plasma, and serially drawn blood samples from inoculated mice (S2.4.1 and S2.4.2). PK parameters (e.g. $C_{max,}$ t_{max}, $t_{1/2}$, AUC) were calculated by non-compartmental approach within WinNonlin software (Pharsight Inc.).

2.5 Cell Culture

Human OS 143B, U2OS, MG63, and SAOS2 cells were obtained from the Duke Cell Culture Facility, which performs routine mycoplasma testing and verifies cell identity by analysis of short tandem repeats. Canine OS Abram’s, D17, and Moresco cell lines were provided courtesy of Dr. Doug Thamm, V.M.D. Colorado State University. The canine OS D418 cell line was developed from a canine OS patient-derived xenograft (Somarelli, Altunel et al. unpublished). The 143B, MG-63, D418, Abrams, D17, and Moresco cells were cultured in standard Dulbecco’s Modified Eagle’s Medium (Thermo-Fisher, Waltham, MA) and the U2OS and SAOS2 lines in

McCoy's 5A Modified Medium (Thermo-Fisher, Waltham, MA). Cells were passed every 2-4 days and were not allowed to reach full confluence.

2.6 Dose-Response Assays of NSPTs on Canine OS Growth.

Dose-dependent effects of NSPTs on all human and canine OS cell-line-growth were determined using a dose-response CellTiter-Glo assay (Promega Corporation, Madison, WI, USA). To do this, 2,500 cells were seeded per well in flat bottomed 96-well plates. 100 µL of media containing either niclosamide in DMSO or NSPTs was added at increasing concentrations (1.6 nM, 8 nM, 40 nM, 200 nM, 1 µM, 5 µM, 25 µM, and 100 µM). Data were compared to a buffer (no drug) control. Cells were incubated at 37 °C for 72 hours and then their cell-viability was assessed using the CellTiter-Glo substrate metabolic end-point assay (Promega, Madison, WI) by addition of 50 µL/well of the CellTiter-Glo substrate. Luminescence was measured with SpectraMax M-series Microplate Reader (Molecular Devices, San Jose, CA). Signal was normalized to the average of untreated (PBS control) wells.

2.7 Western Blot Analysis of Canine Cell Lines.

The ability of NSPTs to modulate signaling pathways known to be dysregulated in OS was investigated by western blotting. A total of 300,000 cells/well of the human OS cell line 143B and patient-derived canine xenograft (D418) cell line were plated and subsequently incubated with a concentration of Niclosamide or NSPTs that were known, from the viability assays, to be on the order of the amount required to reduce cell-viability to almost zero. As shown in the results of the cell viability assay, (shown later in **Figure 3**) this value was at least 20 µM Niclosamide or NSPT. Cells were therefore incubated for 0, 1, 2, 4, and 8 hours with 20 µM Niclosamide or NSPT. Cytosolic and nuclear fractions of lysates at intermediate timepoints were extracted with Radioimmunoprecipitation assay (RIPA) lysis buffer and the Nuclear/cytoplasmic extraction reagent (NE-PER) (Thermo-Fisher, Waltham, MA). Halt Protease and Phosphatase Inhibitor Cocktail was added to both lysis buffers for a final concentration of 2X. Cell lysates were centrifuged at 16,000 g at 4 °C for 15 minutes. Lysate was separated via Nu PAGE 4-12% Bis-Tris SDS-PAGE and transferred onto nitrocellulose membranes. After blocking with Superblock (TBS) Blocking buffer (Thermo-Fisher, Waltham, MA), membranes were incubated with primary antibody overnight at 4 °C and secondary antibody for 1 hour at room temperature. Primary antibodies included anti-pS6 ser235/236 (clone 91B2, 1:1000), anti-S6 (clone 54D2, 1:1000), anti-Notch1 (clone D1E11, 1:1000), anti-Akt (pan) (clone 11E7, 1:1000), anti-pSTAT3 tyr705 (clone D3A7, 1:2000), anti-Histone H3 (clone D1H2, 1:2000), anti-ß-catenin (clone L87A12, 1:1000), anti-pAkt Ser473 (clone 193H12, 1:1000), and anti-STAT3 (clone 123H6, 1:1000) (Cell Signaling Technology, MA). Loading controls included anti-GAPDH (1:5000) (Abcam, MA) and anti-alpha tubulin (1:5000) (Abcam, MA). IRDye 680 nm and 800 nm secondary antibodies were purchased from Li-Cor (Lincoln, NE). Blots were imaged with the Odyssey Fc Imaging System and analyzed using Image Studio software (Li-Cor). Signal was normalized to GAPDH, alpha-tubulin, or Histone H3 loading controls.

2.8 Isolation of NLS mCherry-Labeled Human and Canine OS Clones

Nuclear Localizing Signal (NLS) mCherry-labeled 143B human and D418 canine OS cell reporters were isolated for *in vitro* multiplexed measurements of the effects of NSPTs on OS

proliferation and apoptosis. Cells were treated with NSPT at the following concentrations: 1.6 nM, 8 nM, 40 nM, 200 nM, 1 μM, 5 μM, 25 μM, and 100 μM. NLS mCherry lentiviral vectors were constructed by the Viral Vector Core, Duke University School of Medicine. Time- and dose-response assays of NSPTs on NLS mCherry labeled 143B human and D418 canine OS cells, representing phase confluence %, used red object fluorescence for cell-count and green object fluorescence for cell area. OS cell lines were plated at 300,000 cells/well onto 6-well plates. Cells were incubated with viral titer (MOI of 5) and polybrene (1:500) for 12 hours. NLS mCherry OS cell lines were then FACS-sorted on a MoFlo Astrios EQ (Beckman Coulter, Brea, CA) sorter using Summit software (Cytomation, Fort Collins, CO). Non-transduced lines were used to determine the fluorescence gating strategy. The upper 50% of NLS mCherry cells were then sorted and a post-sort analysis confirmed purity.

2.9 Live-Cell Imaging for Kinetic Determination of Proliferation and Analysis of Apoptosis.

Live-cell imaging assessment of NSPTs' effects on NLS mCherry labeled human and canine OS proliferation and apoptosis were performed using the IncuCyte® S3 (Essen BioSciences, Ann Arbor, MI) with the DEVD-amino acid (Asp-Glu-Val-Asp motif) substrate (IncuCyte® Caspase-3/7 Green Apoptosis Assay Reagent, Essen BioSciences, Ann Arbor, MI). Cells were treated with the same concentrations of NSPTs (1.6 nM, 8 nM, 40 nM, 200 nM, 1 μM, 5 μM, 25 μM, and 100 μM) for 72 hours. Phase-contrast red and green fluorescence channel images were acquired every 2 hours. IncuCyte® S3 imaging software was utilized to calculate percent confluency, total NLS cell red fluorescence area per well, and total caspase green fluorescence area. Images were assessed for final plots at 96 hours.

2.10 Generation of zsGreen-Labeled Human and Canine OS Clones for PuMA.

To label OS cells with zsGreen, a total of 300,000 HEK293T cells were plated onto 6-well plates in complete DMEM and transfected using Lipofectamine LTX plus at 30% confluence with a vector-mix consisting of 2.0 μg pCL-Ampho, and 2.0 μg pLCNX2 zsGreen construct DNA (CloneTech, Mountain View, CA). Human and canine OS cell lines were plated at 300,000 cells/well onto 6-well plates. Viral supernatant was collected off HEK293T cells and transferred onto adherent mid-log human and canine OS cells using a 0.40 μm CA filter. Transduced human and canine OS cell lines were selected with 100 μg/mL G418 for 14 days.

2.11 Ex vivo Pulmonary Metastasis Assay (PuMA).

The *ex-vivo* Pulmonary Metastasis Assay (PuMA) was utilized as previously described (Mendoza, Hong et al. 2010, Lizardo and Sorensen 2018) to assess the efficacy of NSPTs to inhibit the growth of zsGreen-labeled human (143B) and canine (D418) OS cells in the metastatic pulmonary tumor microenvironment (See Supplemental Text for full description).

2.12 Determination of NSPT maximum tolerable dose

We attempted to determine the single maximal tolerable dose (sMTD) of NSPT for the i.v. route (via tail-vein injection). We carried out a step-wise dose increase with one mouse at the lowest dose and 3 mice per higher doses until any significant impact on mouse behavior was observed over 24 h. C57BL/6 mice (Jackson Laboratory, Bar Harbour, Maine, US) were injected with a

volume of 0.1ml or 0.2 mL or 0.25 mL per dose. At the time of this study, we had not observed any toxicity with an injection of 200 µL (0.2 mL) of a 100 µM concentrated suspension of NSPTs (low dose study (Kerr 2017, Kerr, Mikati et al. 2017)), and so 1 mM NSPT was selected to be the starting injected dose . Again, at the time, the highest achievable dose of the NSPT preparation was 6 mM, and so single 0.1 mL injections of 1 mM and 6mM NSPT were administered to give approximate dosing of 3 mg/kg and 20 mg/kg respectively. Higher target-doses of 36 mg/kg and 47 mg/kg were achieved by increasing the volume of injection of the 6mM suspension to 0.2 mL and 0.25 mL respectively. A single iv dose of NSPT, that did not cause significant behavioral change in behavior of all 3 mice was considered tolerated. As shown in Results, the highest dose was well tolerated and so this dosing did not actually achieve a sMTD.

2.13 Generation of Luciferase-Labeled Human and Canine OS Clones

In order to measure lung-colonization and metastatic tumor growth and development, *in vivo*, in the metastatic mouse model over time we generated Luciferase-labeled human and canine OS clone reporters. These reporter cells provided an accurate and accessible assessment of *in vivo* metastatic tumor burden when animals were administered the luciferin substrate and view by an *In Vivo* Imaging System (Caliper Life Sciences, Inc., PerkinElmer, Waltham, MA). Lentiviral transduction of a luciferase-expressing plasmid was carried out as described above for zsGreen labeling. PCW-107 was a gift from Dr. Kris Wood, PhD. Equivalent luciferase expressing clones were selected via the Dual-Luciferase Reporter Assay System (Promega, Madison, WI).

2.14 Mouse Studies of OS Metastasis at Two NSPT-Dosing Levels

OS tail vein metastasis studies were carried out at two NSPT-dosing levels of 0.59 mg/kg and 50 mg/kg. Luciferase-labeled OS cell lines 143B (Human) and D418 (canine patient-derived) were cultured as described above. Cells were harvested for injection by trypsinization while in mid-log phase of growth (50-80% confluence) and concentrated to $5x10^6$ cells/mL in Dulbecco's phosphate buffered saline (DPBS). Viability was assessed to be >90% by hemocytometer prior to inoculation. Cells were kept at 4 °C until inoculation, which occurred within 2 hours of preparation. Animal studies were performed in accordance with the approved protocols of the Duke University Institutional Animal Care and Use Committee (IACUC).
In this lung-metastasis model, cells were injected by tail vein injection on "Day 0", allowed to reach and start to colonize the lungs for 1 day before NSPT nanoparticles were administered i.v. again by tail vein injection. The model therefore allowed for direct exposure of OS cancer cells that were in the very first and early stages of lung colonization These cells were thus likely to be accessible from the blood stream by the i.v. injection of each 200 µL dose of nanoparticles (0.59 mg/kg or 50 mg/kg). Controls were the same volume of PBS (200 µL) and an intraperitoneal injection of Doxorubicin, 1.2 mg/kg in PBS. Thus, on "Day 0", the OS cell preparations ($1x10^6$ cells in 200 µL PBS) were injected directly into the tail veins of 6-week old SCID ($Prkdc^{scid}$) and beige ($Lyst^{bg}$) mice (Charles River, Wilmington, MA), ~20gms in weight. Then, starting on "Day 1" post-inoculation, mice underwent randomized stratification based on initial pulmonary seeding luminescence and sex. The total number of mice was 50, consisting of 5 mice in each

group. Mice were randomly distributed amongst the following treatment groups: PBS, NSPT, Doxorubicin (low- and high-dose groupings in Supplemental S2.14.1).
Mice were weighed every 3 days and monitored for signs of morbidity as evidence of presumed pulmonary metastases or side effects of treatment. Signs monitored included anorexia, dehydration, dyspnea, diarrhea, lethargy, or decreased grooming activity. In order to produce the tumor cell-luminescence, prior to imaging, mice were injected intraperitoneally with D-Luciferin in 200 µL PBS (GoldBio, St. Louis, MO) at 150 mg/kg. In order to determine time-to-peak luminescence, a kinetic determination of D-Luciferin biodistribution was carried out by serial-imaging mice with known pulmonary disease for 30 minutes following luciferin injection. Results (**Supplementary Figure S5**) showed that peak luminescence was obtained within 15 minutes. Thus, for all subsequent studies, mice were imaged after 15 minutes and the bioluminescence was captured using the IVIS Lumina XR system (Caliper Life Sciences, Inc., PerkinElmer, Waltham, MA). Living Image 4.5 software (Caliper) was used to capture the images and quantify the signal. After mice were euthanized, the thoracic cavities were opened and lungs were perfused with 10% buffered formalin by tracheal injection using a blunt perfusion cannula. Lungs were weighed and examined grossly for the number of visible metastatic lesions on the surface and the left lungs were examined histologically for the number of internal metastases by sectioning and microscopic examination after H&E staining. Ten non-sequential serial sections were examined per animal.

2.15 Statistical Analysis

Results are displayed as mean ± standard error of the mean (SEM), unless otherwise indicated. Luminescence data for the CellTiter-Glo assay that measured ATP and hence cell viability in dose-response experiments, were plotted on a log[concentration] scale and fitted with 4-parameter logistic curves, IC_{50} values, and standard errors were calculated from the curve inflection points. In the 4-parameter logistic model (Sebaugh 2011), the relationship between the concentration of the drug or prodrug (x) and the cell viability (y), is given by the equation that includes the "4 parameters":

$$x = c\left(\frac{a-d}{y-d} - 1\right) \qquad \text{Eqn 1}$$

a = the minimum value that can be obtained (i.e. what happens at 0 dose)
d = the maximum value that can be obtained (i.e. what happens at infinite dose)
c = the point of inflection (i.e. the point on the S shaped curve halfway between a and d)
b = Hill's slope of the curve (i.e. this is related to the steepness of the curve at point c).
One-way ANOVA with Tukey's post hoc multiple comparisons was utilized for pairwise comparisons of PuMA lung tumor burden. Wilcoxon pairwise tests were used to compare *in vivo* bioluminescence data. Statistical analysis for data analyses were performed with JMP Pro (SAS, Cary, NC) with a significance level at $p < 0.05$, unless otherwise indicated. Graphs were plotted on Prism 7 (GraphPad, La Jolla, CA).

3. Results

3.1 Size and Stability of NSPTs in Vitro and Pharmacokinetics (PK)/Stability in Vivo

NSPTs were made for both *in vitro* and *in vivo* studies using the established methods of Hervella et al, (Hervella, Walke et al. 2019). All formulations were evaluated for size stability in water, and also in non-ionic media including, equiosmotic sucrose or glucose, and isotonic PBS. Results showed that all NSPT suspensions, as made, were size-stable at 4 ^{o}C in water, and also in the non-ionic equiosmotic sucrose or glucose or PBS (See **Figure S1A and B, Supplemental Information**). The rapid solvent injection method (Hervella, Walke et al. 2019) gave a suspension concentration of 100 μM for the low-dose sample, and the nanoparticle size (diameter) directly after making was measured by DLS (*intensity* mode) to be 30 ± 5 nm, in close agreement with Hervella et al's results (Hervella, Walke et al. 2019). For the up-concentrated sample, the sizes increased slightly. For all 5 of the 50 mg/kg treatments the *"intensity"* average distribution particle diameter was 45 ± 5 nm. As shown in **Figure 1A**, the intensity average distribution for Treatment 1 was 44.7 nm ± 1.6 nm. Shown in **Figure 1 B** is a scaled schematic of a representative 30nm diameter NSPT. It is shown with a 16.6nm diameter, isotropic, core of niclosamide stearate and a stabilizing lipid monolayer of DSPC:Chol, containing a coverage of polyethylene glycol (PEG) provided by 5 mol% of DSPE-PEG^{2000}. Detailed discussion of this schematic with reference to its critical size and phase-state is reserved for the discussion section.

The niclosamide-stearate is a niclosamide prodrug in which a fatty acid stearate is covalently linked to niclosamide by an ester bond. In vivo, the ester bond is expected to be hydrolyzed by chemical and/or enzymatic hydrolysis, releasing "free" niclosamide. In order to assess the extent of the hydrolysis and the achieved levels of niclosamide in plasma, we performed a pharmacokinetic (PK) experiment in mouse whereas 50 mg/kg NSPT was injected i.v. and plasma collected in time within 24 h. In addition, to learn about the intrinsic stability of NSPT in solution and plasma and to better understand the obtained PK data, 37 ^{o}C incubation of NSPT in PBS, mouse plasma, and human plasma was performed as well.

The **Figure 2B** shows the PK profiles for NSPT (measured as NS) and NIC, both exhibiting single exponential decay of the same half-life ($t_{1/2}$ = 5 h), as calculated from the slope in the log-lin plot (Figure 2B, inset). Dashed line shows the published data obtained after i.v. bolus administration of NIC to rat (Chang et al. 2006). In this experiment by Chang et al, the compound was administered intravenously (i.v.) at a dose of 2-mg/kg. The dosing solution was prepared by dissolving the compound in a mixture of dimethyl sulfoxide (DMSO)/ cremophor EL/water (3/15/82 v/v/v). Interestingly, compared to the Area Under the Curves (AUC) for our Niclosamide Stearate (NS) of 3560h*ug/ml and NIC of 690h*ug/ml, the Chang data (Chang et al. 2006) shows an AUC of only 1.4 h*ug/ml (2,543 times lower than the NS AUC). The inset shows the log-linear plot giving a similar half-life for both NS (5 hrs) and NIC (5.5hrs) by a single-order decay. And for comparison with our study, we see that Chang's direct injection has a similar half-life of 5.7 hrs albeit at much lower plasma levels.

We dose-adjusted and plotted the data to illustrate the magnitude of the gain in NIC exposure (AUC) when NIC is administered not in its free form but rather as NSPT ($AUC_{NSPT->NIC}/AUC_{free\ NIC}$ = 470). The NSPT and NIC are of different size and physical properties so the observed PK profile of the released NIC in plasma may be explained as being rate-controlled by the rate of NSPT loss from circulation (as observed from similar nano-particles, $t_{1/2}$ ~7 h, Hervella, Dam et al. 2018), whereas the magnitude of the NIC plasma concentration is determined by the rate of NIC production from NSPT by enzymolysis. Indeed, the Figure 2A shows the *in-vitro* production of NIC by a mixed order enzymolysis process (fast first-order followed by slower

zero-order) in mouse plasma as being of the same order of magnitude, $t_{1/2}$ ranging from 2-13 h. The Figure 2A also reveals that the rate of enzymolysis in human plasma is very similar as in mouse plasma, whereas the simple pH-dependent hydrolysis in aqueous solution (PBS) is much slower as expected for lipid monolayer-protected NSPT core.

3.3 Cell viability, proliferation, and ATP present in human and canine OS Cells in vitro

NSPTs inhibited cell viability, proliferation, and the quantity of intracellular-ATP present in human and canine OS Cells *in vitro*. As shown in **Figure 3A** for the human 143B and canine D418 cell lines, dose response assays demonstrated that both niclosamide (from DMSO) and NSPTs (added as an aqueous suspension) inhibited *in vitro* canine and human OS cell-growth in a dose-dependent manner. (See **Supplementary Figure S2A** for individual plots of all 8 cell lines**).** Also, the dose response for cell viability gave very similar profiles for both the parent drug niclosamide and the niclosamide stearate prodrug therapeutic nanoparticles for both the canine and human cells.

Cumulated in **Figure 3B**, IC_{50} values for all cell lines were in the micromolar to sub-micromolar range, showing, in general, that all cells were slightly more sensitive to Niclosamide from DMSO when compared to NSPTs (Mean IC_{50}: 0.57 µM vs. Mean IC_{50}: 1.22 µM, respectively; p=0.002). However, on average, there were no statistically significant differences between inhibition of human and canine OS cells by niclosamide and NSPTs (Mean IC_{50}: 1.16 µM vs. Mean IC_{50}: 1.27 µM, respectively; p=0.79).

Figure 3C shows time- and dose-response assays of NSPTs in terms of a proliferation-assay based on NLS mCherry labeled 143B human and D418 canine OS cells. **Figure 3C (i)**, compares cell count and cell area representing phase confluence %. Below about 5 µM NSPT, cells showed increasing confluence and hence proliferation as total red area **Figure 3C (ii)**. Above 5 µM there was a marked dose-dependent inhibition in cell proliferation in both cell lines. When plotted in **Figure 3D**, the micromolar IC_{50} of NSPTs for this live-cell imaging assay of proliferation (**Figure 3A**) were similar to the IC_{50} for the cell viability (ATP based end point) assay **Figure 3C (ii)** for canine OS cells (mean IC_{50} proliferation 3.46 µM vs. mean IC_{50} viability: 1.27 µM, respectively; p=0.009), but were somewhat greater for human (Mean IC_{50} proliferation: 6.74 µM vs. Mean IC_{50} viability: 0.88 µM, respectively; p=0.17). The green fluorescence intensity assay (**Figure 3C (iii)**) measured the response of the cells to NSPTs in terms of effective apoptosis. Here, the half maximal effective concentrations (EC_{50s}) of NSPTs on caspase 3/7 facilitated-apoptosis in both 143B and D418 OS cells showed clear evidence of apoptosis in a dose dependent manner. (See **Supplementary Figure S2B and C** for individual plots of all 8 cell lines**)**

As shown in the cross plots in **Figure 3D**, cell proliferation was inhibited with increasing NSPT addition and the level of measured apoptosis rose. The EC_{50s} for apoptosis though were significantly higher than the IC_{50s} for inhibition of proliferation (mean EC_{50} apoptosis: 20.9 µM vs. mean IC_{50} proliferation: 4.868 µM, p=0.04). (See **Supplementary Figure S2D** for individual plots of all 8 cell lines**).** Time-dependent inhibition of proliferation by NSPTs was noted as quickly as 4 hours after initiation of treatment in the relatively high concentration, 100 µM, groups. In these same high concentration, 100 µM, groups Caspase 3/7 mediated apoptosis was first noted 12 hours after initiation of treatment. Thus, there appears to be a slight non-apoptotic,

cytotoxic inhibition of OS cells when treated with lower concentrations and at earlier exposure times. The results of the Western Blots are shown in **Figure 3E** for both cell lines, as presented next.

3.4 NSPTs inhibited multiple human and canine OS signaling pathways

Multiple signaling pathways have been implicated in niclosamide's growth inhibition of human and canine OS cells (Pan, Ding et al. 2012), including NF-κB, Wnt/β-catenin, Notch, ROS, mTORC1, and Stat3, and so we expected, and tested to determine if and to what extent NSPTs would do the same. The PI3K/Akt/mTOR/S6 signaling pathway, and particularly the downstream mammalian target of rapamycin (mTOR) and complex (mTORC1), are important regulators of cell-cycle progression and are frequently abnormally activated in OS (Ding, Congwei et al. 2016). Increasing mTOR activity has been shown to drive cell cycle progression and increase cell proliferation. Conversely, as was shown in cervical cancer cells (Li, Li et al. 2013), the inhibition of mTOR (by the inhibitor AZD8055, at only 10 nM) inhibits proliferation and glycolysis, and, again, was found to induce apoptosis in the HeLa cells in a time-dependent manner. In the same study by Li et al, the phosphorylation of the C1 substrates p70S6K and phosphorylation of the mTORC2 substrate Akt were deregulated. An inhibition of mTOR in OS cells could therefore correlate with their reduced proliferation (**Figure 3 C**). As shown in **Figure 3E**, in both 143B **(i)** and D418 (**(ii)** NSPTs induced a time-dependent reduction in the phosphorylated form of S6. Notably, in the D418 cell line, an initial increase in the p-Akt signal was observed at 1 hour before the signal decreased. The nuclear localization of β-catenin (**Figure 3E (iii)** was reduced in separate cell lysates in 143B using nuclear/cytoplasmic fractionation of untreated and treated cells. The presence of nuclear β-catenin was also reduced in the 143B cell lines after 24 hours of treatment with 20 μM niclosamide-stearate nanoparticles. As shown in **Supplementary Figure S3A and B** for individual plots of all 8 cell lines**,** nuclear β-catenin also reduced in MG-63, U2OS and SaOS2 cell lines after the same 24 hours of treatment with NSPT.

Taking all 8 cell lines into consideration, (See **Supplementary Figure S3A and B** for individual plots of all 8 cell lines**),** the amount of phosphorylated Akt did not change over 8 hours in Abrams and Moresco cell lines. As with the 143B, D418 lines, NSPTs also induced a time-dependent reduction in the phosphorylated form of S6 in MG-63, U2OS, SaOS2, D17, and Moresco. Phosphorylated STAT3 increased initially in MG-63, U2OS, SaOS2, and D17 before decreasing at 8 hours, while it was not present at all in the other human and canine OS cells (See **Supplementary Figure S3A and B)**. Niclosamide's inhibition of the Akt/mTOR/S6 pathway is particularly beneficial, as mTOR/p70S6K has been clinically prognostic of disease-free and overall survival in patients presenting with primary OS (Zhou, Deng et al. 2010). Regarding the PI3K/Akt/mTOR/S6 pathway, NSPTs increased phosphorylated Akt but only transiently over the first two hours.

3.5 NSPTs decreased ex vivo growth of pulmonary metastases

To interrogate the ability of NSPTs to slow the progression of pulmonary metastases in 143B human and D418 canine OS cells, we performed an *ex vivo* Pulmonary Metastasis Assay (PuMA) (Mendoza, Hong et al. 2010, Lizardo and Sorensen 2018), (See also **Supplementary**

Figure S4 for images of lung slices loaded with OS cancer cells prepared ex vivo after tracheotomy as well as Bright-field-Fluorescent images of lung metastases in the lung tissues ex-vivo on Day 1 (400ms exposure) at 5X magnification and a Higher magnification (40X) image of fluorescent lung metastases). PBS control, doxorubicin, or NSPTs, were administered to the lung slices upon plating out on the day of surgery. The fluorescence results of the PuMA (quantified as mean fluorescence area/total lung area) are shown in **Figure 4.** For the PBS controls, both 143B (**A)** and D418 (**B)** cells established bulky, metastatic disease by Day 5 and continued to develop through Day 10.

Interestingly, the tumor burden was more prevalent at the initial stages (Day 1 and 5) in the 143B human cell line as quantified in **Figure 4B**) than in the D418 canine as quantified in **Figure 4D**. For example, on Days 1 and 5 the 143B human cell line showed increasing tumor burden of 0.018, 0.042, while, in contract the D418 tumor burden started out at 0.0125 on Day 1, and only increased slightly to 0.014 on Day 5. However, while the 143B on Day 10 had actually reduced slightly to 0.035, the D418 line increased dramatically to 0.06 by Day 10.

For the drug-treated slices, all dosing (Dox and NSPTs) was, as expected, relatively ineffective on Day 1. Satisfyingly though, NSPTs, at both 10 μM and 50 μM, were able to completely reduce the lung tumor burden to undetectable by Day 5 in both 143B human (**Figure 4A, B, C**) and D418 canine (**Figure 4D, E, F**) OS cells. The standard of care chemotherapeutic, doxorubicin, also significantly inhibited lung tumor burden at 1 μM and 10 μM concentrations, although, morphologically and quantitatively, there was a higher tumor burden in both cell lines at Day 5 (**Figure 4B** and **C**, **D** and **F** respectively)). By day 10, NSPTs continued to show complete reduction of tumor burden with no evidence of recovery, and the doxorubicin response had become morphologically and quantitatively similar to NSPT.

Thus, in the *ex vivo* Pulmonary Metastasis Assay we found that the assay accurately recreated the growth of 143B human and D418 canine OS cells, (that we had seen for controls in cell culture media as proliferation (**Figure 3Ci**)), but now within an actual lung tumor microenvironment. They also effectively showed the inhibitory effects of NSPTs when dosed in the culture dish medium through 1-2 mm thick lung parenchyma. Interestingly, the amounts of NSPTs that were effective in both 143B and D418 cell lines in the PuMA, when related to the IC_{50}s for cell viability from cell culture (0.71 and 1.6 μM), showed that NSPTs (10 μM by day 5) were able to massively inhibit the growth of pulmonary metastases in this model at only 14x and 6x the IC_{50}, for cell viability (ATP inhibition), respectively.

3.6 NSPTs administration to determine toxicity

The first feasibility study was carried out at a modest 0.59 mg/kg and no deleterious effects were seen in the mice in terms of toxicity or regarding weight loss over the first 30 days (**Figure 5D**), until they succumbed to the lung metastases. We therefore decided to increase the dose and provide some measure of an MTD by carrying out a dose escalation and observing any response in C57BL/6 mice over 24hrs. As shown in **Table 1. Parameters for Dose escalation study**, three dosing levels were tested. The initial plasma concentrations achieved in the mice were not measured, but were calculated based on a mouse blood volume of 1mL (Riches, Sharp et al. 1973, NC3Rs 2019).

An NSPT injection into a C57BL/6 mouse of 100 μL of a 1 mM suspension concentration (equivalent to a 3.21 mg/kg dose and 91 μM NSPT in the blood stream), produced no changes in behavior when followed for 24 hours after injection. Similarly increasing the 100 μL injection concentration to a 6 mM suspension of NSPTs, (providing ~20 mg/kg and a blood concentration of 541μM), also showed no adverse effects during 24hr inspection in the 3 C57BL/6 mice. Because 6mM NSPTs was a relative upper concentration limit to our preparation at the time (including ultrafiltration for up-concentration), in order to achieve a higher dose, 200 μL, 250 μL, and 250 μL were injected into each of three subsequent mice (to give 36.81 mg/kg, 45.77 mg/kg, and 47.24 mg/kg, equivalent to blood concentrations of 0.99 mM, 1.19 mM, and 1.19 mM respectively). Again, there were no adverse effects at 24hrs.

Therefore, the MTD was apparently not reached even at 50 mg/kg with up to 1.19 mM of the prodrug Niclosamide Stearate (and therefore Niclosamide) in the blood stream. We therefore used this much higher dose for the second metastatic assay experiment. The result was, that NSPTs can be administered to mice at 50mg/kg without discernable toxicity.

3.7 In vivo studies at two dosings in a mouse model of OS metastasis

Two dosings of NSPTs were trialed. The first dose was at 0.59 mg/kg and was used as a safe and exploratory feasibility study of the possible effects of the new NSPTs in the lung metastasis model (Kerr 2017). Following the dose escalation study, where we had determined that a 50mg/kg dose could be achieved without any discernable toxicity (and so was not even yet the MTD), the second study was carried out at this dose of 50 mg/kg NSPTs (Reddy 2018). To simulate the effect of metastatic disease, mice were inoculated via tail-vein injection with 5×10^5 luciferase-labeled 143B human or D418 canine PDX-derived OS cells (as depicted schematically in **Figure 5E**). This injection produced a colonization of the lung with OS cells as disseminated metastases. Data for each study are now presented below.

3.7.1 NSPTs at 0.59mg/kg low dose study

NSPTs at 0.59 mg/kg prolonged the survival in 143B-bearing mice without the treatment-derived morbidity shown by Doxorubicin. In the low dose study (Kerr 2017), a cohort of sixteen 12-week-old SCID/beige mice bearing the 143B tumor line were treated in groups with either weekly i.v. doses of: the control of 200 μL PBS; or 200 μL doses of niclosamide-stearate nanoparticles in PBS suspension at a molar concentration of 100 μM (0.059 mg/mL); or weekly intraperitoneal (i.p.) doses of doxorubicin at 1.2 mg/kg in PBS; or combination therapy (niclosamide-stearate nanoparticles i.v. weekly, doxorubicin i.p. weekly). As shown in **Figure 5**, they were followed for 50 days for overall survival, and for 17 days using IVIS imaging to observe and quantitate tumor burden. Mice were euthanized when they presented with signs of significant morbidity, such as lethargy or behavioral changes due to the lung metastatic burden. IVIS images in **Figure 5A**, representing a typical example of the results, showed that the PBS control mice rapidly developed lung metastases within 7 days, and by day 16 there was massive lung tumor burden visible.

In contrast, both NSPT- and Dox-treated mice showed reduced tumor burden compared to these controls. However, the NSPT cohort showed consistently less tumor burden than the

Doxorubicin-treated cohort. This visual data was quantified in **Figure 5B**, giving the tumor burden as average bioluminescence in units of Radiance "photons/second/cm^2/steradian" (p/s/cm^2/sr) (see footnote[1]). The Dox and NSPT cohorts had a lower bioluminescence than controls with NSPTs being the least, signifying their lower tumor burden out to day 17. Thus, in mice that were inoculated with the human 143B cell line, treatment with niclosamide-stearate nanoparticles at this first dose of 0.59mg/kg was associated with delayed tumor growth compared to the saline-treated group, with significantly less tumor burden at 14 and 16 days ($p=0.0367$, $p=0.020$ respectively). Note: this 0.59 mg/kg dose represents a calculated blood concentration (based on a mouse weight of 20 g and a 1mL mouse blood volume), of 20 μM; this is 12x the measured cell viability IC_{50} (of 1.68 μM) for this 143B cell line from **Figure 3** (see later in Discussion).

In the Kaplan-Meier analysis, (**Figure 5C**), at the point at which all the PBS control mice had died, NSPT-treated mice were still at 100% survival. The 0.59 mg/kg NSPT treatment, given only on a weekly basis, prolonged survival with a mean survival of 40 days compared to 30 days in the PBS group ($p=0.0067$, **Figure 5C**). There was actually no statistically significant difference in survival between the mice treated with niclosamide-stearate nanoparticles, doxorubicin, or combined therapy. Importantly though for this 143B human cell line, unfortunately, mice had to be euthanized early for the Doxorubicin cohort. The doxorubicin-treated mice developed diarrhea and weight loss early in the course of therapy (**Figure 5D**) and doxorubicin treatment was held for both doxorubicin-only and combined-therapy groups at day 21. The NSPT and PBS treated groups did not demonstrate any early treatment-related side effects or weight loss out to at least 30 days, until they succumbed to the cancer.

3.7.2 NSPTs at 50 mg/kg high dose study

NSPTs at 50 mg/kg inhibited metastatic development in D418-bearing mice and safely delayed tumor progression. In this higher dose study (Reddy 2018), 6-week old SCID/beige mice were again inoculated via tail-vein injection with luciferase-labeled D418 canine PDX-derived OS cells (as shown schematically in **Figure 5E**). (See **Supplemental Table S1** for details of each mouse in the study, showing mouse weight (g), NPST diameter (nm), suspension concentration (mM), and amount (mg) of NPST injected in each 200 mL to achieve 50mg/kg niclosamide Stearate (equivalent to 27mg/kg niclosamide) per mouse dosing).

Animals were treated with either the control of phosphate-buffered saline (PBS) or NSPTs by i.v injection, or doxorubicin intraperitoneally (i.p.). In this experiment, mice were relocated in the microscopy suite and so bioluminescence by IVIS was measured from Day 0. As shown in **Figure 6B**, immediately following inoculation, OS cells were seen to be trapped in the lungs and

[1] As described by Caliper Life Sciences Inc, Sciences, C. L. (2011). "Image Display and Measurement." Retrieved 9th February, 2019, from https://mbi-ctac.sites.medinfo.ufl.edu/files/2017/02/Concept-Tech-Note-2-Image-Display-and-Measurement.pdf."the radiance unit of photons/sec/cm2/sr is the number of photons per second that leave a square centimeter of tissue and radiate into a solid angle of one steradian (sr). A steradian can be thought of as a three-dimensional cone of light emitted from the surface that has a unit solid angle. Much like a radian is a unit of arc length for a circle, a steradian is a unit of solid angle for a sphere. An entire sphere has 4π steradians. Lens systems typically collect light from only a small fraction of the total 4π steradians".

gave an initial seeding-bioluminescence that was not significantly different between treatment groups.

The seeding value decreased rapidly in PBS controls from 34525 ± 24796 p/s/cm^2/sr value to 1766 ± 535 p/s/cm^2/sr at day 3, presumably, as cancer cells failed to survive and colonize. From day 10 though, the bioluminescence and hence tumor burden rapidly increased reaching levels of 30,000 p/s/cm^2/sr, but now representing established metastases in the lungs. Interestingly, based on the IVIS images, in contrast to the 143B experiment (**Figure 5A**), control mice inoculated with the same number (5 x 10^5 luciferase-labeled) D418 OS cells took longer to develop the lung metastases (Compare **Figure 5A** day 16 with **Figure 6A** day 17).
Importantly, as shown in **Figure 6B**, the lung tumor burden for mice treated with the NSPTs on only a weekly basis (Days 1 and 8, 15, 22, 29), began to diverge from the PBS group at Day 9, and remained at the ~2,000 p/s/cm^2/sr bioluminescence baseline-level out to 26 days, before rising slightly by the endpoint at Day 32. This demonstrated for the first time that weekly dosing of NSPTs at 50mg/kg prevented the establishment and control metastatic disease in the lungs of the D418 cells. The result was even more significant in view of the data that showed this particular tumor was actually resistant to the standard of care drug, doxorubicin (**Figure 6B**). Again, as with the lower 0.59mg/kg dose cohort, NSPT-treated mice at 50mg/kg did not have any weight loss associated with five weekly doses. Importantly for this drug (niclosamide) that has shown to be relatively non-toxic in cell studies to healthy cells, even at this relatively large i.v. 50 mg/kg dose, NSPT-treated mice had significantly greater body weight when compared against doxorubicin-treated mice, as shown in **Figure 6C**, and even gained weight while on the dosing regimen.

4. Discussion

Taken together, our data suggest NSPT is a novel and effective formulation of niclosamide ready to undergo further evaluation as a new treatment for OS. Analysis of the potential mechanism of action of this NSPT pinpointed multiple pathways known to be deregulated in OS. Interestingly, other literature (Park, Shin et al. 2011, Jurgeit, McDowell et al. 2012, Sukumar and Gopinath 2016, Alasadi, Chen et al. 2018, Childress, Alexopoulos et al. 2018) as well as our own data *in vitro* indicate niclosamide, at its most fundamental level, acts by disrupting ATP synthesis. As such, this mechanism acts upstream of many of the other processes in the OS cell, since they require ATP and phosphorylation to operate. Mechanistically, from a medicinal chemistry point of view, this activity of niclosamide represents a drug target that is not the usual drug-protein (or -DNA -RNA) macromolecule but may well be action at the lipid membrane level. In support of this hypothesis niclosamide has been described as a proton shunt in mitochondria, and these effects induce OS-cell kill by apoptosis (Jurgeit, McDowell et al. 2012, Alasadi, Chen et al. 2018). This brings into play a new kind of medicinal chemistry for drugability, i.e., designing better lipophilic anions (a delocalized electron in relatively high logP-molecule) capable of even more efficient membrane partitioning and proton carrier functions to dissipate the pH gradients in mitochondria, lysozomes and other internal cell organelles that rely on cation gradients.

Cell signaling studies for active components of the mTOR, Jak/STAT, and Wnt/β-catenin pathways, showed that, in both human and canine OS, NSPTs decreased the phosphorylated form of S6 (pS6) at 8 hours without any decrease in phosphorylated Akt. The PI3K/Akt/mTOR/S6 signaling pathway, and particularly the downstream mammalian target of rapamycin (mTOR) and complex (mTORC1), are important regulators of cell cycle progression and are frequently activated abnormally in OS (Ding, Congwei et al. 2016). Niclosamide's inhibition of the Akt/mTOR/S6 pathway is particularly beneficial, since mTOR functions as a sensor of mitogen, energy and nutrient levels, and is a central controller of cell growth and a negative regulator of autophagy. The mTOR/p70S6K axis has been clinically prognostic of disease-free and overall survival in patients with primary OS (Zhou, Deng et al. 2010). In the D418 and D17 cell lines, while p-Akt was found to increase with treatment, the downstream decrease in p-S6 is likely due to direct inhibition of either mTORC1 or p70S6K.

In vivo we observed significant reductions in metastatic burden and improved survival in mice with metastatic OS at a low dose of just 0.59 mg/kg weekly. Following this positive "low-dose" data, we next used a dose of 50mg/kg and found no increase in toxicity. While niclosamide itself when given orally is extremely safe (WHO 2002)), this is the first time that such a high dose of 50 mg/kg NSPT has been injected i.v., to obtain an initial dosing of 27 mg/kg equivalent niclosamide. For this particular drug (niclosamide and the prodrug NSPTs) the issue is therefore not reducing toxicity, as it is in many chemotherapy applications, but more effective drug delivery (than oral dosing). Thus, in these experiments and with this NSPT design, the goal of bioavailable dosing had been achieved and, moreover, the NSPTs were efficacious in preventing metastatic disease without systemic toxicity.

When compared to the oral dosing in the clinical trial for prostate cancer of Schweizer et al (Schweizer, Haugk et al. 2018) that gave sub-micromolar plasma concentrations that were not even close to the *in vitro* efficacy our high-micromolar values are approximately 10,000 times the values achieved by oral dosing. Even in the prospective phase II clinical trial of niclosamide in patients with metastasized colorectal cancer (mCRC) (Burock, Daum et al. 2018, Burock, Daum et al. 2018) the median C_{max} plasma levels of 0.665 µg/mL (~2 µM), our values for NSPT are still almost 1,000 times the ones achieved with an oral dosing of 2 g/patient. This shows how extremely significant is of our new NSPT-based i.v. dosing approach to the cancer treatment by niclosamide.

We demonstrated here an innovative strategy to engage the principles of medicinal chemistry to repurpose an old, economical drug. We managed to optimize it for drug delivery as a unique nanoparticle formulation (Chen 2016), that increased the bioavailability of niclosamide in the blood stream (by i.v. injection of the prodrug at 50 mg/kg) and allowed its validation in the preclinical setting in mice with a well-performing lung metastasis-model of OS. Using bioluminescent tumor labeling, we were able to study and establish the *in vivo* efficacy of the NSPTs in both a human OS cell line (143B) and a canine cell line (D418). The data suggest that 30 nm diameter NSPTs are both effective and safe in treating simulated metastatic disease for both human and canine OS in an *in vivo* mouse model. The NSPT nanoparticles were designed to be stable against hydrolysis, due to the tight lipid-cholesterol monolayer, and "stealthy", i.e., they contained enough DSPE-PEG^{2000} on their surfaces embedded in the DSPC:cholesterol monolayer that coated the particle to provide a relatively long (6-7hrs) circulation half-life for the prodrug compound. Currently there are no other options for administering niclosamide i.v. preclinically except from a direct DMA injection (Bhattacharyya, Ren et al. 2017) which is

clinically unacceptable. Our pro-drug delivery strategy converted the relatively water-insoluble niclosamide (Sw = 4μM) to its even less soluble (~30nM) stearate ester for the expressed purpose of making injectable NSPT nanoparticles at doses at least as high as 50mg/kg. This strategy has successfully transformed a previously unacceptably-low-bioavailable niclosamide into a customizable and efficacious therapeutic with the requisite pharmacokinetics and tolerability profile for immediate canine and subsequent human clinical testing. NSPTs are able to inhibit OS cell growth in several orthogonal modalities (IC50 = 0.2 μM – 2 μM) and function as effective prodrug therapeutics in metastatic OS *in vivo*, leading to decreased metastatic tumor burden *ex vivo* and *in vivo*. Future directions will be multilateral and involve several areas of interest. Perhaps the most important from a biological and interaction standpoint is further elucidating the broad mechanisms of NSPTs and indeed niclosamide on OS cells and other solid tumors. In addition, this would be helpful in then determining an *in vivo* pharmacokinetic marker of NSPT action. Different nanoparticle formulations (ligand-targeting, fluorescent tagging, active immunomodulation, etc.) and combinations with established and candidate chemotherapeutics and concentrations can be trialed in high throughput *in vitro* and *ex vivo* PuMA screens. Validating a primary orthotopic model that can spontaneously metastasize would then provide another opportunity to test NSPTs effectiveness in a complementary model. Finally, pilot clinical testing in canine patients with primary and metastatic OS would provide valuable, actionable insight into the viability and challenges with NSPT production, drug quality assurance, and clinical administration and subsequent tolerability observations. From those early clinical studies, additional clinical studies can be escalated to larger canine, randomized control trials and human Phase I studies to realize the ultimate goals of improving survival and decreasing morbidity for OS patients.

6. Acknowledgements

This work was funded by a Hyundai Hope on Wheels Award.

7. References Cited

Ahmed, K., H. V. Shaw, A. Koval and V. L. Katanaev (2016). "A Second WNT for Old Drugs: Drug Repositioning against WNT-Dependent Cancers." Cancers **8**(7): 66.

Alasadi, A., M. Chen, G. V. T. Swapna, H. Tao, J. Guo, J. Collantes, N. Fadhil, G. T. Montelione and S. Jin (2018). "Effect of mitochondrial uncouplers niclosamide ethanolamine (NEN) and oxyclozanide on hepatic metastasis of colon cancer." Cell Death & Disease **9**(2): 215.

Aljubran, A. H., A. Griffin, M. Pintilie and M. Blackstein (2009). "Osteosarcoma in adolescents and adults: survival analysis with and without lung metastases." Ann Oncol **20**(6): 1136-1141.

Arend, R. C., A. I. Londoño-Joshi, J. M. Straughn and D. J. Buchsbaum (2013). "The Wnt/β-catenin pathway in ovarian cancer: A review." Gynecologic Oncology **131**(3): 772-779.

Arslanagic, A., P. Hervella, K. Glud, J. Mollenhauer and David Needham (2016). Characterization of targeted and non-targeted uptake in breast cancer stem cells of triple negative origin. CLINAM, Basel, Switzerland.

Arslanagic-Kabiljagic, A. (2019). Establishing the feasibility for endogenous delivery of pure-drug anti-cancer nanoparticles in the treatment of metastatic breast cancer disease. PhD, University Southern Denmark.

Bhattacharyya, J., X. R. Ren, R. A. Mook, J. B. Wang, I. Spasojevic, R. T. Premont, X. H. Li, A. Chilkoti and W. Chen (2017). "Niclosamide-conjugated polypeptide nanoparticles inhibit Wnt signaling and colon cancer growth." Nanoscale **9**(34): 12709-12717.

Biermann, J. S., W. Chow, D. R. Reed, D. Lucas, D. R. Adkins, M. Agulnik, R. S. Benjamin, B. Brigman, G. T. Budd and W. T. Curry (2017). "NCCN guidelines insights: bone cancer, version 2.2017." Journal of the National Comprehensive Cancer Network **15**(2): 155-167.

Burock, S., S. Daum, U. Keilholz, K. Neumann, W. Walther and U. Stein (2018). "Phase II trial to investigate the safety and efficacy of orally applied niclosamide in patients with metachronous or sychronous metastases of a colorectal cancer progressing after therapy: the NIKOLO trial." BMC cancer **18**(1): 297-297.

Burock, S., S. Daum, H. Tröger, T. D. Kim, S. Krüger, D. T. Rieke, S. Ochsenreither, K. Welter, P. Herrmann, A. Sleegers, W. Walther, U. Keilholz and U. Stein (2018). "Niclosamide a new chemotherapy agent? Pharmacokinetics of the potential anticancer drug in a patient cohort of the NIKOLO trial." Journal of Clinical Oncology **36**(15_suppl): e14536-e14536.

Chen, M., J. Wang, J. Lu, M. C. Bond, X.-R. Ren, H. K. Lyerly, L. S. Barak and W. Chen (2009). "The Anti-Helminthic Niclosamide Inhibits Wnt/Frizzled1 Signaling." Biochemistry **48**(43): 10267-10274.

Chen, W., Mook, jr., Robert A. Wang, Jiangbo, Ren, Xiu-Rong, Chen, Minyong, Barak, Lawrence S., Lyerly, Herbert Kim, and Needham, David. (2016). Chemical modulators of signaling pathways and therapeutic use. D. University. **PCT/US16/39295**.

Childress, E. S., S. J. Alexopoulos, K. L. Hoehn and W. L. Santos (2018). "Small Molecule Mitochondrial Uncouplers and Their Therapeutic Potential." Journal of Medicinal Chemistry **61**(11): 4641-4655.

Crawford, S. (2013). "Is it time for a new paradigm for systemic cancer treatment? Lessons from a century of cancer chemotherapy." Frontiers in Pharmacology **4**(68).

Ding, L., L. Congwei, Q. Bei, Y. Tao, W. Ruiguo, Y. Heze, D. Bo and L. Zhihong (2016). "mTOR: An attractive therapeutic target for osteosarcoma?" Oncotarget **7**(31): 50805.

Ebbesen MF, B. J., P Natalini, A Elie, D Needham (2019). "Solubility of Niclosamide and its binding to albumin as a function of pH predicts uptake and accumulation in lysosomes and lipid droplets in cancer cell cultures." in preparation.

EPA (1999). Niclosamide United States Prevention, Pesticides EPA-738-F99-013, Environmental Protection And Toxic Substances, Agency (7508C).

Eward, W., S. Steve, D. Needham and J. Somarelli (2018). Testing a New Prodrug Nanoparticle Formulation of Niclosamide as a Novel Therapy for Osteosarcoma. NC State University and Duke UNiversity, Consortium for Canine Comparative Oncology, the College of Veterinary Medicine at NC State University and the Duke Cancer Institute.

Ferrari, S., P. Ruggieri, G. Cefalo, A. Tamburini, R. Capanna, F. Fagioli, A. Comandone, R. Bertulli, G. Bisogno and E. Palmerini (2012). "Neoadjuvant chemotherapy with methotrexate, cisplatin, and doxorubicin with or without ifosfamide in nonmetastatic osteosarcoma of the extremity: an Italian sarcoma group trial ISG/OS-1." Journal of clinical oncology **30**(17): 2112-2118.

Friebele, J. C., J. Peck, X. Pan, M. Abdel-Rasoul and J. L. Mayerson (2015). "Osteosarcoma: A Meta-Analysis and Review of the Literature." Am J Orthop (Belle Mead NJ) **44**(12): 547-553.

824 Hervella, P., P. Walke, A. Arslanagic, C. Azevedo, T. Ulven, M. Ebbesen and D. Needham (2019). "A New
825 Niclosamide Stearate Prodrug Therapeutic of the Re-appropriated Anti-Cancer Drug Niclosamide: Formulation,
826 Size Distribution, and Chemical Stability Against Hydrolysis and Enzymolysis." to be submitted to J Pharm Sci.

827 Jin, Y., Z. Lu, K. Ding, J. Li, X. Du, C. Chen, X. Sun, Y. Wu, J. Zhou and J. Pan (2010). "Antineoplastic
828 mechanisms of niclosamide in acute myelogenous leukemia stem cells: inactivation of the NF-κB pathway and
829 generation of reactive oxygen species." Cancer research **70**(6): 2516-2527.

830 Jurgeit, A., R. McDowell, S. Moese, E. Meldrum, R. Schwendener and U. F. Greber (2012). "Niclosamide Is a
831 Proton Carrier and Targets Acidic Endosomes with Broad Antiviral Effects." PLOS Pathogens **8**(10): e1002976.

832 Kadri, H., O. A. Lambourne and Y. Mehellou (2018). "Niclosamide, a Drug with Many (Re)purposes."
833 ChemMedChem **13**(11): 1088-1091.

834 Kager, L., A. Zoubek, U. Potschger, U. Kastner, S. Flege, B. Kempf-Bielack, D. Branscheid, R. Kotz, M. Salzer-
835 Kuntschik, W. Winkelmann, G. Jundt, H. Kabisch, P. Reichardt, H. Jurgens, H. Gadner and S. S. Bielack (2003).
836 "Primary metastatic osteosarcoma: presentation and outcome of patients treated on neoadjuvant Cooperative
837 Osteosarcoma Study Group protocols." J Clin Oncol **21**(10): 2011-2018.

838 Kansara, M., M. W. Teng, M. J. Smyth and D. M. Thomas (2014). "Translational biology of osteosarcoma." Nature
839 Reviews Cancer **14**(11): 722-735.

840 Karimi, L. (2019 (exp)). Preclinical Characterization and In vitro Cell Testing of Novel Niclosamide Nanoparticle
841 Formulations for Treatment of Prostate Cancer. PhD, SDU.

842 Karthika, S., T. K. Radhakrishnan and P. Kalaichelvi (2016). "A Review of Classical and Nonclassical Nucleation
843 Theories." Crystal Growth & Design **16**(11): 6663-6681.

844 Kerr, D., L (2017). A novel formulation of niclosamide treats metastatic osteosarcoma in vivo. MD MD, Duke
845 University, School of Medicine.

846 Kerr, D. L., H. Mikati, A. Tovmasyan, W. Chen, P. Walke, R. T. Kreulen, J. Somarelli, S. B. Dewitt, T. Camp, J.
847 Herbert, D. S. Hsu, B. Brigman, G. Hanna, G. Palmer, D. Needham and W. Eward (2017). A novel formulation of
848 niclosamide treats metastatic osteosarcoma in vivo. Connective Tissue Oncology Society, Maui, Hawaii.

849 Li, S., Y. Li, R. Hu, W. Li, H. Qiu, H. Cai and S. Wang (2013). "The mTOR inhibitor AZD8055 inhibits
850 proliferation and glycolysis in cervical cancer cells." Oncology letters **5**(2): 717-721.

851 Li, Y., P.-K. Li, M. J. Roberts, R. C. Arend, R. S. Samant and D. J. Buchsbaum (2014). "Multi-targeted therapy of
852 cancer by niclosamide: A new application for an old drug." Cancer Letters **349**(1): 8-14.

853 Li, Y., P. K. Li, M. J. Roberts, R. Arend, R. S. Samant and D. J. Buchsbaum (2014). "Multi-targeted therapy of
854 cancer by niclosamide: a new application for an old drug." Cancer letters **349**(1): 8-14.

855 Li, Z., Y. Yu, S. Sun, B. Qi, W. Wang and A. Yu (2015). "Niclosamide inhibits the proliferation of human
856 osteosarcoma cell lines by inducing apoptosis and cell cycle arrest." Oncology reports **33**(4): 1763-1768.

857 Liao, Z., G. Nan, Z. Yan, L. Zeng, Y. Deng, J. Ye, Z. Zhang, M. Qiao, R. Li, S. Denduluri, J. Wang, Q. Wei, N.
858 Geng, L. Zhao, S. Lu, X. Wang, G. Zhou, H. H. Luu, R. C. Haydon, T. C. He and Z. Wang (2015). "The
859 Anthelmintic Drug Niclosamide Inhibits the Proliferative Activity of Human Osteosarcoma Cells by Targeting
860 Multiple Signal Pathways." Curr Cancer Drug Targets **15**(8): 726-738.

Liu, C., W. Lou, C. Armstrong, Y. Zhu, C. P. Evans and A. C. Gao (2015). "Niclosamide suppresses cell migration and invasion in enzalutamide resistant prostate cancer cells via Stat3-AR axis inhibition." The Prostate **75**(13): 1341-1353.

Lizardo, M. and P. Sorensen (2018). "Practical Considerations in Studying Metastatic Lung Colonization in Osteosarcoma Using the Pulmonary Metastasis Assay." Journal of visualized experiments: JoVE(133).

Londono-Joshi, A. I., R. C. Arend, L. Aristizabal, W. Lu, R. S. Samant, B. J. Metge, B. Hidalgo, W. E. Grizzle, M. Conner, A. Forero-Torres, A. F. Lobuglio, Y. Li and D. J. Buchsbaum (2014). "Effect of niclosamide on basal-like breast cancers." Mol Cancer Ther **13**(4): 800-811.

Marina, N. M., S. Smeland, S. S. Bielack, M. Bernstein, G. Jovic, M. D. Krailo, J. M. Hook, C. Arndt, H. van den Berg and B. Brennan (2016). "Comparison of MAPIE versus MAP in patients with a poor response to preoperative chemotherapy for newly diagnosed high-grade osteosarcoma (EURAMOS-1): an open-label, international, randomised controlled trial." The Lancet Oncology **17**(10): 1396-1408.

Mehta, M. (2016). Biopharmaceutics Classification System (BCS): Development, Implementation, and Growth., Wiley.

Mendoza, A., S.-H. Hong, T. Osborne, M. A. Khan, K. Campbell, J. Briggs, A. Eleswarapu, L. Buquo, L. Ren, S. M. Hewitt, E.-H. Dakir, S. Garfield, R. Walker, G. Merlino, J. E. Green, K. W. Hunter, L. M. Wakefield and C. Khanna (2010). "Modeling metastasis biology and therapy in real time in the mouse lung." The Journal of Clinical Investigation **120**(8): 2979-2988.

Mialou, V., T. Philip, C. Kalifa, D. Perol, J. C. Gentet, P. Marec-Berard, H. Pacquement, P. Chastagner, A. S. Defaschelles and O. Hartmann (2005). "Metastatic osteosarcoma at diagnosis: prognostic factors and long-term outcome--the French pediatric experience." Cancer **104**(5): 1100-1109.

Mirabello, L., R. J. Troisi and S. A. Savage (2009). "Osteosarcoma incidence and survival rates from 1973 to 2004." Cancer **115**(7): 1531-1543.

Morse, M. (2017). A phase I study: A Study of Niclosamide in Patients With Resectable Colon Cancer (Pro00066964). Duke University Medical Center.

Nagarajan, R., A. Kamruzzaman, K. K. Ness, V. G. Marchese, C. Sklar, A. Mertens, Y. Yasui, L. L. Robison and N. Marina (2011). "Twenty years of follow-up of survivors of childhood osteosarcoma." Cancer **117**(3): 625-634.

NC3Rs. (2019). "Decision tree." Retrieved 6th Feb 2019, from https://www.nc3rs.org.uk/mouse-decision-tree-blood-sampling.

NCI. (2014). "NCI DTP (Developmental Therapeutics Program, NCI 60 Screening Results." from (https://dtp.cancer.gov/services/nci60data/colordoseresponse/jpg/758440).

Needham, D., A. Arslanagic, K. Glud, P. Hervella, L. Karimi, P.-F. Høeilund-Carlsen, K. Kinoshita, J. Mollenhauer, E. Parra and A. Utoft (2016). "Bottom up design of nanoparticles for anti-cancer diapeutics:“put the drug in the cancer’s food”." Journal of drug targeting **24**(9): 836-856.

Osada, T., M. Chen, X. Y. Yang, I. Spasojevic, J. B. Vandeusen, D. Hsu, B. M. Clary, T. M. Clay, W. Chen, M. A. Morse and H. K. Lyerly (2011). "Antihelminth Compound Niclosamide Downregulates Wnt Signaling and Elicits Antitumor Responses in Tumors with Activating APC Mutations." Cancer Research **71**(12): 4172-4182.

Pan, J.-X., K. Ding and C.-Y. Wang (2012). "Niclosamide, an old antihelminthic agent, demonstrates antitumor activity by blocking multiple signaling pathways of cancer stem cells." Chinese Journal of Cancer **31**(4): 178-184.

900 Pan, J. X., K. Ding and C. Y. Wang (2012). "Niclosamide, an old antihelminthic agent, demonstrates antitumor
901 activity by blocking multiple signaling pathways of cancer stem cells." Chin J Cancer **31**(4): 178-184.

902 Park, S. J., J. H. Shin, H. Kang, J. J. Hwang and D.-H. Cho (2011). "Niclosamide induces mitochondria
903 fragmentation and promotes both apoptotic and autophagic cell death." BMB Rep. **44**(8): 517-522.

904 Perera, D. R., K. A. Western and M. G. Schultz (1970). "Niclosamide* Treatment of Cestodiasis." The American
905 Journal of Tropical Medicine and Hygiene **19**(4): 610-612.

906 Reddy, G. B. (2018). Utilizing a Novel Formulation of Niclosamide to Treat Metastatic Human and Canine
907 Osteosarcoma MD MD, Duke University School of Medicine.

908 Riches, A. C., J. G. Sharp, D. B. Thomas and S. V. Smith (1973). "Blood volume determination in the mouse." The
909 Journal of physiology **228**(2): 279-284.

910 Schweizer, M. T., K. Haugk, J. S. McKiernan, R. Gulati, H. H. Cheng, J. L. Maes, R. F. Dumpit, P. S. Nelson, B.
911 Montgomery, J. S. McCune, S. R. Plymate and E. Y. Yu (2018). "A phase I study of niclosamide in combination
912 with enzalutamide in men with castration-resistant prostate cancer." PLOS ONE **13**(6): e0198389.

913 Sciences, C. L. (2011). "Image Display and Measurement." Retrieved 9th February, 2019, from https://mbi-
914 ctac.sites.medinfo.ufl.edu/files/2017/02/Concept-Tech-Note-2-Image-Display-and-Measurement.pdf.

915 Sebaugh, J. L. (2011). "Guidelines for accurate EC50/IC50 estimation." Pharmaceutical Statistics **10**(2): 128-134.

916 So Jung, P., lt, sup, gt, lt, sup, gt, S. Ji Hyun, lt, sup, gt, lt, sup, gt, K. Hee, lt, sup, gt, lt, sup, gt, H. Jung Jin, lt, sup,
917 gt, lt, sup, gt, amp, amp, C. Dong-Hyung, lt, sup, gt, lt, sup and gt (2011). "Niclosamide induces mitochondria
918 fragmentation and promotes both apoptotic and autophagic cell death." BMB Rep. **44**(8): 517-522.

919 Sukumar, U. K. and P. Gopinath (2016). "Field-actuated antineoplastic potential of smart and versatile PEO-bPEI
920 electrospun scaffold by multi-staged targeted co-delivery of magnetite nanoparticles and niclosamide-bPEI
921 complexes." RSC Advances **6**(52): 46186-46201.

922 Suliman, M. A., Z. Zhang, H. Na, A. L. L. Ribeiro, Y. Zhang, B. Niang, A. S. Hamid, H. Zhang, L. Xu and Y. Zuo
923 (2016). "Niclosamide inhibits colon cancer progression through downregulation of the Notch pathway and
924 upregulation of the tumor suppressor miR-200 family." International journal of molecular medicine **38**(3): 776-784.

925 Taran, S. J., R. Taran and N. B. Malipatil (2017). "Pediatric osteosarcoma: an updated review." Indian journal of
926 medical and paediatric oncology: official journal of Indian Society of Medical & Paediatric Oncology **38**(1): 33.

927 Walke, P. (2018). Physico-Chemical Parameters of Nanoparticles that Govern Prodrug Design and Application in
928 Anticancer Nanomedicine. PhD, Unnversity of Southern Denmark (SDU).

929 Walke, P. B., P. Hervella and D. Needham (2017). Lipid-Coated Stealth Nanoparticles of Novel Hydrophobic
930 Prodrug, Niclosamide Stearate, as Cancer Therapeutic: Formulation and Physico-Chemical Characterization of
931 Nanoparticles. 6th International Pharmaceutical Federation Pharmaceutical Sciences World Congress, Stockholm,
932 Sweden.

933 Whelan, J., S. Bielack, N. Marina, S. Smeland, G. Jovic, J. Hook, M. Krailo, J. Anninga, T. Butterfass-Bahloul and
934 T. Böhling (2014). "EURAMOS-1, an international randomised study for osteosarcoma: results from pre-
935 randomisation treatment." Annals of oncology **26**(2): 407-414.

936 WHO (2002). WHO Specifications and Evaluations for Public Health Pesticides: Niclosamide, World Health
937 Organisation, Geneva.

WHO (2017). "The selection and use of essential medicines: report of the World Health Organization (WHO) Expert Committee." World Health Organization technical report series(1006): i.

Ye, T., Y. Xiong, Y. Yan, Y. Xia, X. Song, L. Liu, D. Li, N. Wang, L. Zhang and Y. Zhu (2014). "The anthelmintic drug niclosamide induces apoptosis, impairs metastasis and reduces immunosuppressive cells in breast cancer model." PloS one **9**(1): e85887.

Zhigaltsev, I. V., Nathan Belliveau, Ismail Hafez, Alex K. K. Leung, Jens Huft, Carl Hansen, and Pieter R. Cullis (2012). "Bottom-Up Design and Synthesis of Limit Size Lipid Nanoparticle Systems with Aqueous and Triglyceride Cores Using Millisecond Microfluidic Mixing." Langmuir **28**(7): 3633-3640.

Zhou, Q., Z. Deng, Y. Zhu, H. Long, S. Zhang and J. Zhao (2010). "mTOR/p70S6K signal transduction pathway contributes to osteosarcoma progression and patients' prognosis." Medical oncology **27**(4): 1239-1245.

8. Tables

	Dose 1		Dose 2				Dose 3		
	Mouse 1		Mouse 1	Mouse 2	Mouse 3		Mouse 1	Mouse 2	Mouse 3
Conc injected NSPT, mM	1		6	6	6		6	6	6
Conc injected NSPT, mg/mL [1]	0.59		3.53	3.53	3.53		3.53	3.53	3.53
Injection volume, mL	0.1		0.1	0.1	0.1		0.2	0.25	0.25
Mouse weight, g	18.5		17	17.5	18		19.2	19.3	18.7
Injected NSPT mg/mouse	0.06		0.35	0.35	0.35		0.71	0.88	0.88
Injected dose, mg/kg	3.21		20.79	20.19	19.63		36.81	45.77	47.24
Blood concentration, μM [2]	90.91		541.17	541.17	541.17		992.14	1190.56	1190.56

[1] ***Calculated based on 593.58 g/mol molar mass of Niclosamide stearate.***

[2] ***Calculated based on a mouse blood volume of 1mL.***

Table 1. Parameters for Dose escalation study. The concentration that the Injected Dose achieves in the C57BL/6 mouse in units of μM is calculated based on a 1ml mouse blood volume. (NOTE: actual plasma volumes/mouse were based on 60 mL/kg, and so were 1.08, 0.99, 1.02, 1.05, 1.12, 1.13, 1.09 mL) (Riches, Sharp et al. 1973, NC3Rs 2019).

9. Figure Legends

FIGURE 1. Nanoparticle size and the Composition and Structure of the NSPT. A) Diameters of nanoparticles measured by DLS directly after making using the rapid solvent injection method. The particle size (hydrodynamic diameter) was measured using a Dynamic Light Scattering instrument (Dyna Pro Nanostar, Wyatt Technology). For all 5 of the 50 mg/kg treatments was 45 ± 5 nm. As shown the DLS algorithm reports three peaks with % Intensity values: Peak 1: 2.2 nm (2.3%); Peak 2: 30.8 nm (92.2%); Peak 3: 414.4 nm (5.4%). Mean PDI for Treatment 1 was 0.303. Shown is the DLS intensity distribution for Treatment 1 of the high dose (50 mg/kg) samples used for D418 tumors. DLS intensity distributions, peaks, PDI, and % intensity for treatments 1 to 5 are shown in **Supplemental Information Figure S1**. **B)** Schematic representation drawn to scale, of an NSPT. The core is represented as an isotropic liquid or solid amorphous material of niclosamide stearate with a lipid monolayer of DSPC:Chol (45:50 mol:mol) providing a mechanical barrier to water penetration and protein binding, and a 5 mol% of DSPE-PEG^{2000} providing a steric barrier to protein binding around the niclosamide stearate core that is depicted here as an amorphous core (it may instead be crystalline, but that is yet to be fully confirmed). Also shown are the dimensions of each of the chemical structures (van der Waals surface) and size of the components, DSPC (3.1 nm), Chol 1.9 nm), DSPE-PEG^{2000}, (DSPE 3.1 nm, and PEG 3.6 nm, making a total size of 6.7 nm) and niclosamide stearate (3.0 nm)

FIGURE 2. *In-vitro* stability and Pharmacokinetics of the Niclosamide Stearate Prodrug Therapeutic (NSPT) . A) Concentration of niclosamide (NIC) generated by hydrolysis and/or enzymolysis of niclosamide stearate (NS) core within NSPT (lipid coated nanoparticles) in PBS, ($t_{1/2}$ = 17 days) and mouse and human plasma (($t_{1/2}$ = >24hrs)) measured versus time for 0.25, 1, 4, and 24 hrs at 37^{o}C, starting with 1.8 mM NS as NSPT. This is equivalent to the estimated zero-time plasma concentration *in vivo* after bolus administration of dose of 50 mg/kg NSPT (27

mg/kg niclosamide equivalent). **B)** Concentration of NS and NIC in plasma measured over 24 h after i.v. administration of 50 mg/kg NSPT (27 mg/kg niclosamide equivalent). The Area Under the Curves (AUC) are: NS, 3560h*ug/ml; and NIC, 690h*ug/ml. Plotted also are published NIC dosed i.v. at 2mg/kg by dissolving the niclosamide in a mixture of dimethyl sulfoxide (DMSO)/ cremophor EL/water (3/15/82 v/v/v) in rat data (dashed) for illustration purposes (Chang et al. 2006) showing an AUC of only 1.4 h*ug/ml and a half-life of 6.7 ± 2.0 hr. Inset is the log-linear plot illustrating the similar half-life for both NS (5 hrs) and NIC (5.5hrs) by a single-order decay.

FIGURE 3. **In Vitro cell viability, proliferation, apoptosis and Western blots**
A) Dose-response assays for niclosamide in DMSO and NSPTs in canine OS cell lines: 143B and D418. (See **Supplementary Figure S2A** for individual plots of all 8 cell lines**)**. **B)** Cumulated IC_{50} values for all human (143B, MG63, U2OS, SaOS2) and canine (D417, Moresco, Abrams, D17) cell line by treatment. **C)** Time- and dose- response assays of NSPTs on NLS mCherry labeled 143B human and D418 canine OS cells, representing: phase confluence % (C(i)); red object fluorescence cell count (C(ii)); and green object fluorescence area (C(iii)) representative of caspase 3/7-dependent apoptotic events. (See **Supplementary Figure S2B and C** for individual plots of all 8 cell lines**)**. **D)** Cross plots for D(i) 143B and D (ii) D418 of Total red area and Normalized green fluorescent intensity vs NSPT concentration at 96 hrs. (See **Supplementary Figure S2D** for individual plots of all 8 cell lines**)**. **E)** Western blot signaling pathway analysis performed on (i) human OS cell line 143B and (ii) patient-derived canine xenograft (D418) Cells were incubated with 20 μM NSPTs for 0-8 hours. (iii), Western blots performed on the 143B cell line after no treatment or treatment with niclosamide-stearate nanoparticles (20 μM) for 24 hours. (See **Supplementary Figure S3A and B** for individual plots of all 8 cell lines**)**.Cell lysates were separated into cytoplasmic and nuclear fractions using ThermoFisher's NE-PER kit and samples were run on 4-12% BT gels, transferred to PVDF membranes and stained with antibodies to β-catenin, tubulin (cytoplasmic loading control) and Histone H3 (nuclear loading control).

FIGURE 4. The *ex vivo* Pulmonary Metastasis Assay (PuMA). (A and D) Representative fluorescence images of pulmonary metastasis assay at 5X magnification with BF and EGFP filter sets (**A**) in human 143B and (B) in canine D418 from days 1, 5, and 10 following exposure to PBS, doxorubicin, and NSPTs. Exposure time was determined daily by PBS control fluorescence intensity. Dosing was done on the first day. (**B and E**) Quantification of lung tumor burden (**B**) in 143B, and (**E**) in D418 using mean fluorescence area over total lung area. (**C and F**) Time-dependent change in treatment group lung tumor burden normalized to daily PBS lung tumor burden for (**C**) 143B and (**F**) D418. Note: these graphs represent normalized lung tumor burden. They are normalized to PBS lung tumor burden for each time point. The treatment groups are always referenced to that day's PBS. That's why the PBS graph appears to not change while the treatment decreases. ns. **p<0.01 vs. PBS, ***p<0.001 vs. PBS, #p<0.05 vs. Dox 10 μM.

FIGURE 5. Low dose (0.59mg/kg) in vivo study. 6-week old SCID/beige mice were inoculated on Day 0 with luciferase-labeled 143B (5×10^5 OS cells and treated with 0.59mg/kg weekly starting on Day1. Animals were injected weekly with 200μl of PBS or 200μl of a 100 μM suspension NSPTs, or Doxorubicin, weekly at 1.2 mg/kg in PBS intraperitoneal. **A)**

Luminescent images for PBS, NSPT, and Dox versus time in a typical example. **B)** Average bioluminescence tumor burden in units of $p/s/cm^2/sr$ for each treatment group versus days post inoculation for the first 17 days (error bars indicate standard error). **C)** Kaplan Meier survival curves for each treatment group with log-rank test comparing PBS, NSPT, doxorubicin, and combination therapy (NSPT + Dox). Mice were also observed for signs of adverse effects including anorexia, dehydration, dyspnea, diarrhea, lethargy, or decreased grooming activity. **D)** Average change in weight by treatment group versus days post inoculation for the first 39 days. **E)** Schematic showing how Luciferase positive tumor cells were delivered to mice by tail-vein injection, adapted from Mendoza et al, (Mendoza, Hong et al. 2010). Statistical significance: *p<0.05 vs. PBS; #p<0.05 vs. Doxorubicin; *p<0.05 PBS vs. Doxorubicin; $p<0.05 NSNP vs. Doxorubicin; #p<0.05 PBS vs. NSPT+Doxorubicin; %p<0.05 NSNP vs. NSPT+Doxorubicin.

FIGURE 6. High does (50 mg/kg) in vivo study. 6-week old SCID/beige mice were inoculated on Day 0 with 5×10^5 luciferase-labeled D418 OS cells and treated with 100 μL of PBS, 100 μL of a (e.g.) 8.44 mM suspension of NSPTs dosed weekly starting on Day 1 or i.p. doxorubicin 1.2mg.kg (MTD) weekly. **A**) Luminescent images for PBS, NSPT and Dox versus Day after inoculation (Note: first dose taken up by the entrapped OS cells). **B**) Average bioluminescence tumor burden for each treatment group versus time (grey PBS, red Dox, teal-green NSPT) with error bars indicating standard error. **C)** Average change in weight by treatment group versus days post inoculation for the first 32 days. Mice were also observed for signs monitored included anorexia, dehydration, dyspnea, diarrhea, lethargy, or decreased grooming activity.

10. Figures

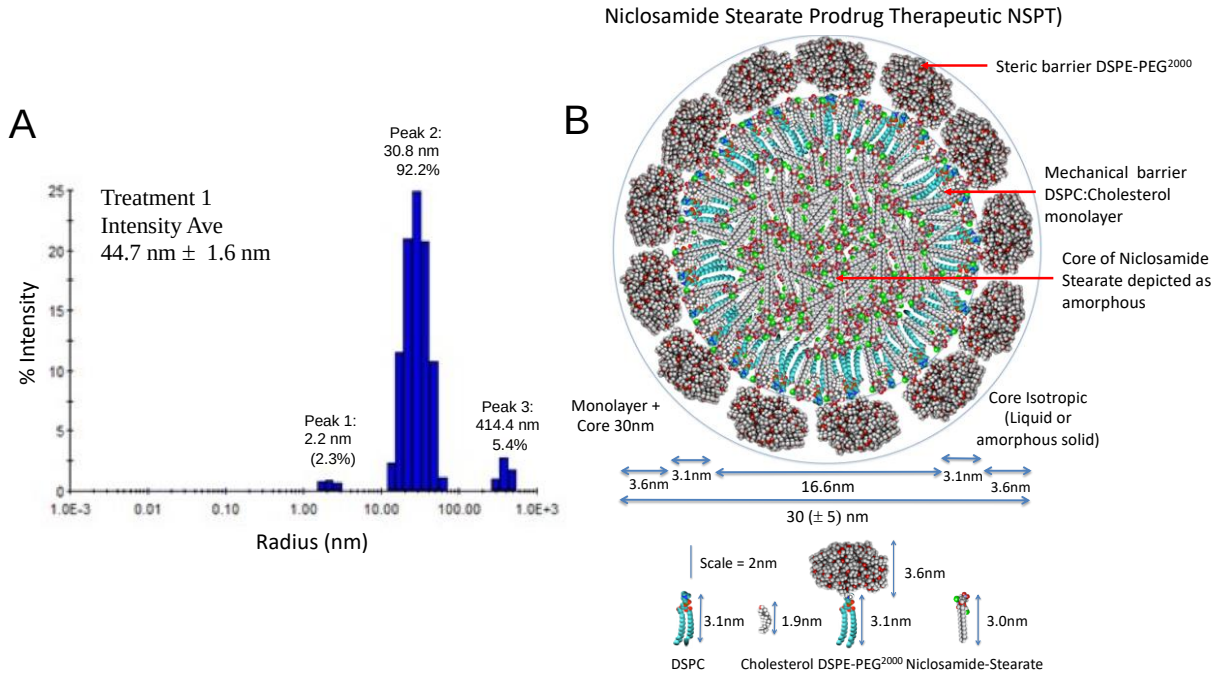

FIGURE 1.

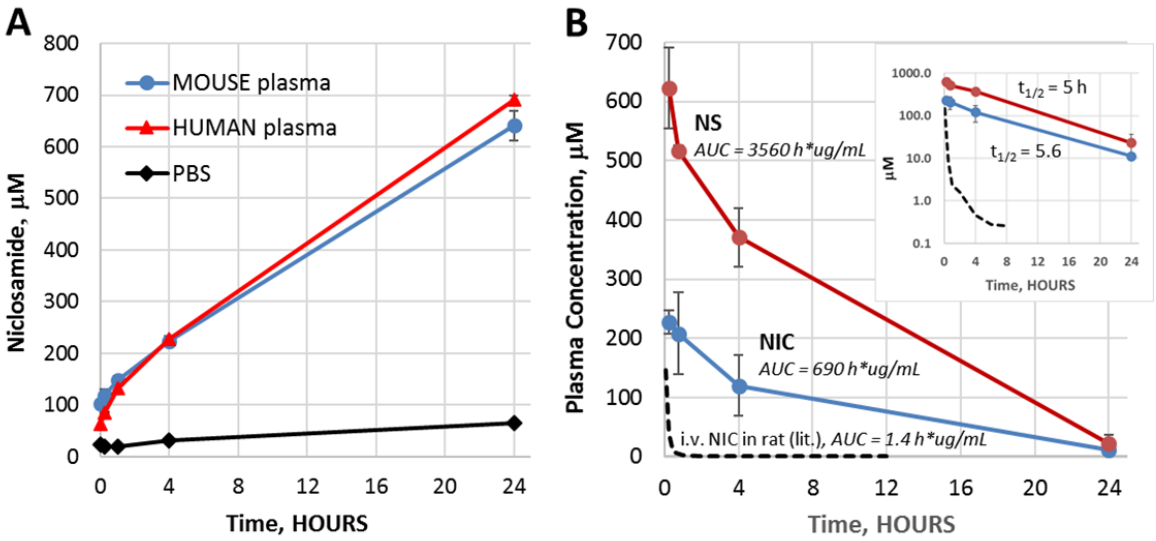

FIGURE 2.

Author Manuscript Published OnlineFirst on May 5, 2020; DOI: 10.1158/1535-7163.MCT-19-0689
Author manuscripts have been peer reviewed and accepted for publication but have not yet been edited.

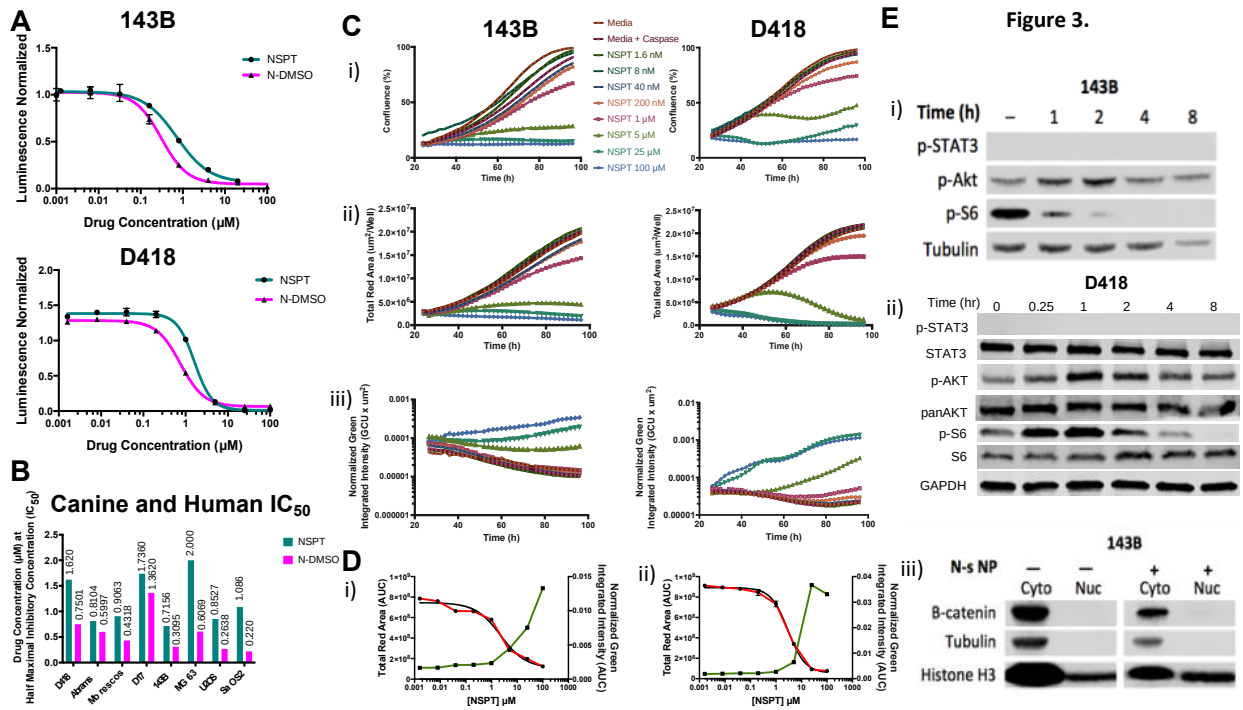

FIGURE 3.

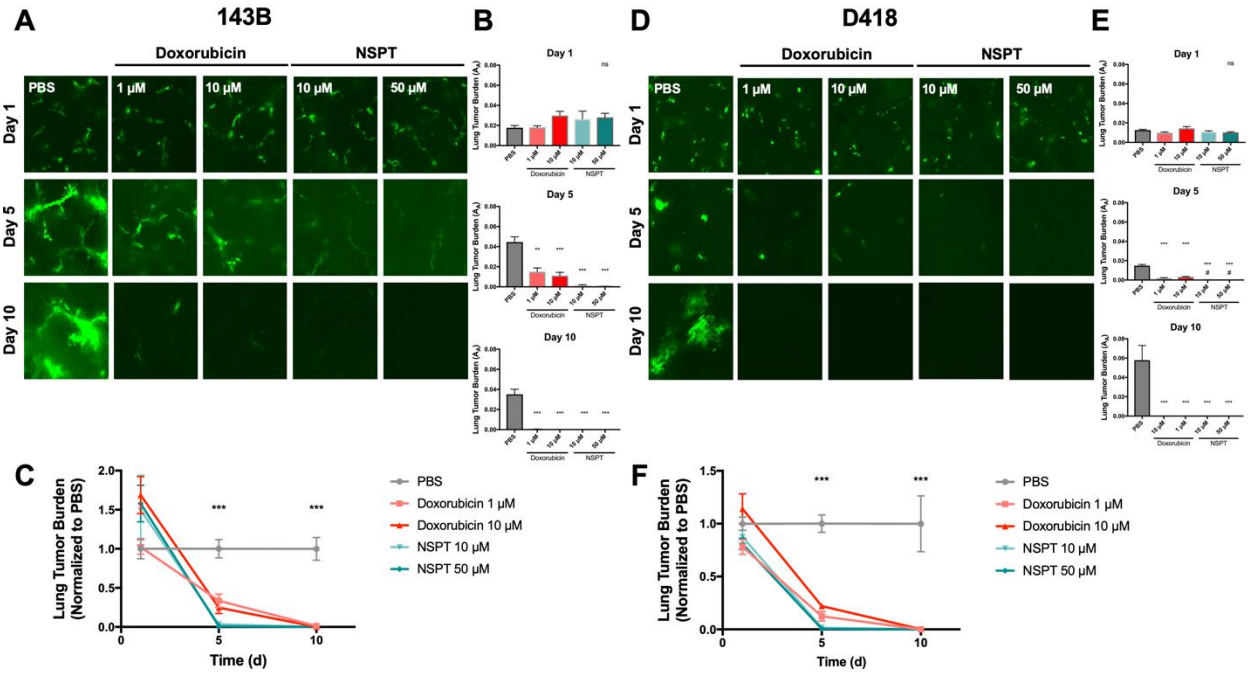

FIGURE 4.

Author Manuscript Published OnlineFirst on May 5, 2020; DOI: 10.1158/1535-7163.MCT-19-0689
Author manuscripts have been peer reviewed and accepted for publication but have not yet been edited.

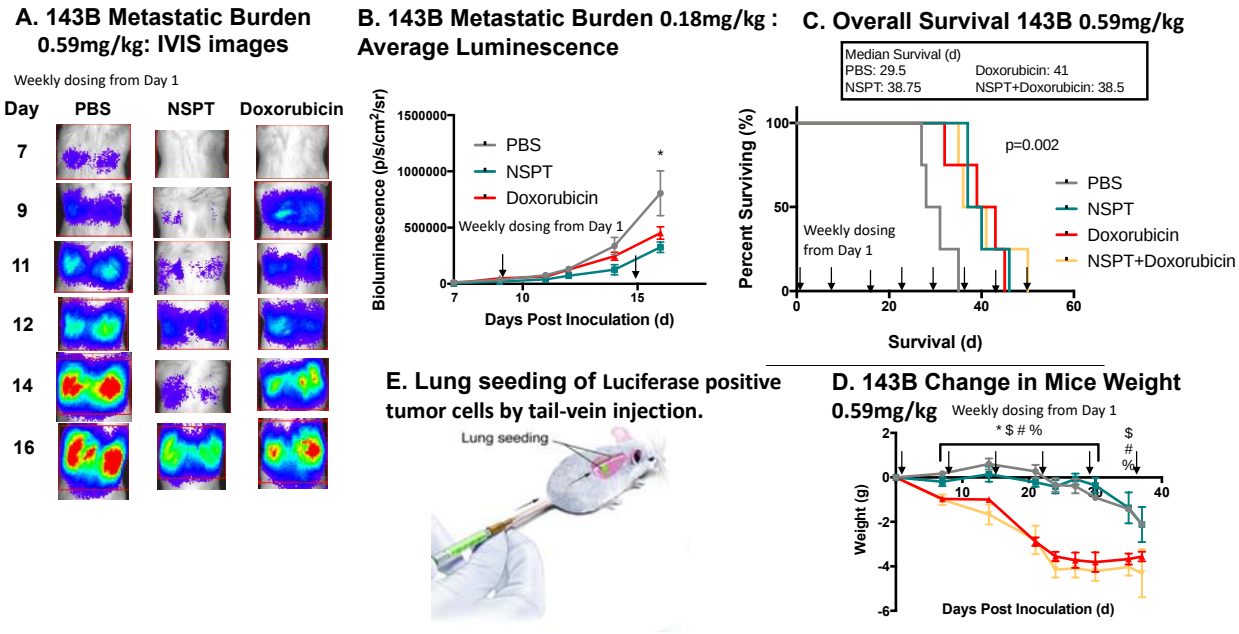

FIGURE 5.

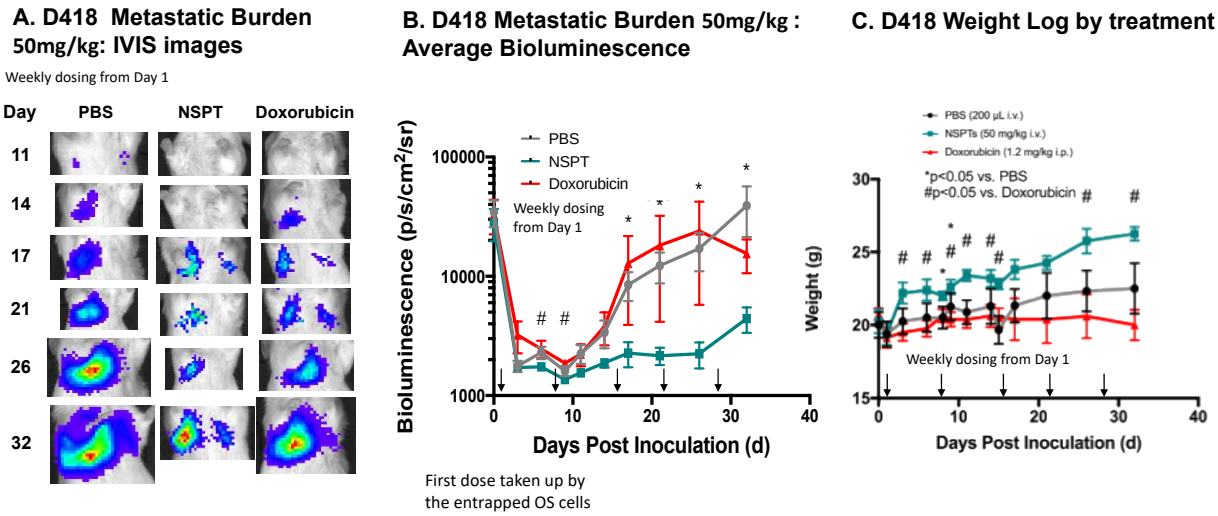

FIGURE 6.

AACR American Association for Cancer Research

Molecular Cancer Therapeutics

Preclinical Testing of a Novel Niclosamide Stearate Prodrug Therapeutic (NSPT) shows efficacy against Osteosarcoma

Gireesh B Reddy, David L Kerr, Ivan Spasojevic, et al.

Mol Cancer Ther Published OnlineFirst May 5, 2020.